Fluorescence Image and Spectrum in Random Media and Cancer Cells

by

Zhiwei Zang

A dissertation submitted to the Graduate Faculty in Engineering in partial fulfillment of the requirements for the degree of Doctor of Philosophy, the City University of New York

1995

This manuscript has been read and accepted for the Graduate Faculty in Engineering in satisfaction of the dissertation requirements for the degree of Doctor of Philosophy.

8/2/95

Date

Chair of Examining Committee

Professor Samir A. Ahmed

8/2/95

Date

Executive Officer

Professor Gerard Lowen

Supervisory Committee

Prof. Fred Moshary

Prof. Mohamed Ali

Prof. Leonid Royman

Dr. Basile Panoutsopoulos

The City University of New York

Abstract

Fluorescence Image and Spectrum in Random Media
and Cancer Cells

by

Zhiwei Zang

Advisor: Professor Samir A. Ahmed

This thesis investigates (1) The capability of using a fluorescence-absorption technique to image objects hidden in scattering media, (2) The effect of multiple light scattering and self absorption on the fluorescence and excitation spectra of dye in random media, and (3) DNA ploidy measurements in breast and colon cancer using fluorescence image cytometry.

To see an object hidden in or behind a highly scattering random medium is one of the most challenging physics and engineering problems. Many different techniques have been introduced for this purpose. In this thesis we introduce an exceedingly simple, yet novel and important technique, fluorescence-absorption technique to improve our ability to see through a highly scattering random medium. Since a luminescent object to be detected in a typical medical application, such as a breast tumor is itself constituted from a highly scattering medium, the effect of scatter on the emitted

luminescence spectra itself is of interest to the further development of these techniques. This is of particular importance since the distribution of the luminescent spectrum itself may relate to medical conditions to be diagnosed. We presents here the results of experiments to examine the impact of internal multiple scattering within a luminescent body on the luminescence spectrum observed at the surface.

New research and development opportunities and advances are evident in the multidisciplinary field of computer-aided microscopy for cell and tissue imaging and analysis. This growth applies to both the development of new and improved scientific method as well as to the utilization of these techniques to investigate significant biomedical applications. Much of the core and supporting technology in this work involves optical and visual process. We, with The Mount Sinai Hospital, measured DNA ploidy for the cancer cells diagnosis research.

Acknowledgement

I would like to express my gratitude to my mentor, Professor Samir A. Ahmed, and the members of the examining committee, Prof. Fred Moshary, Prof. Mohammed Ail, Prof. Leonid Roytman, Prof. Gerard Lowen, and Dr. Basile Panoutsopoulos.

My thanks to Prof. K.M. Yoo, Prof. Joseph Barba, and my fellow students at the Laser and remote sensing Laboratory.

This thesis study was made possible from the educational and financial support provided in part by the Department of Electrical Engineering of the City College of the City University of New York.

TABLE OF CONTENTS

LIST OF FIGURES

I. Introduction

1.1 Background

Imaging through a thick random scattering medium has many potential practical applications such as seeing an airplane through a cloud and detecting a tumor hidden in human breast. The ballistic photons which traverse through the medium in a straight line path and the early arriving diffuse photons which traverse through the medium almost in the same direction as the ballistic light carry the image information, while the diffuse photons contribute the background noise.

Light scattering in random medium is common in nature, such as sun light being scattered in the cloud, and room light being scattered in the wall paint. Transport theory, multiple scattering theory, and the diffusion approximation are used to describe the light scattering in random medium.[1] When light enters a disordered scattering medium, it is inevitably scattered randomly in all directions. The degree of light scattering depends on the spatial distribution and time variation of the dielectric constant (index of refraction) of the medium. The gross properties of light scattering by a random medium are characterized by three key parameters: the scattering mean free path l_s, the transport mean free path l_t, and the absorption length l_a. The scattering mean free path l_s is the mean distance between scatterings. $l_s = 1/(n\sigma_s)$, where n is the number density of the scatterer in the medium, and σ_s is the scattering cross-section of a single scatterer. The scattering cross-section depends on the shape of the particle, the size of the particle with respect to the wavelength of the light, and the refractive index of the particle with respect to the background. The total scattering cross section σ_s is related to the differential scattering cross section $\sigma(\theta,\phi)$ by:

$$\sigma_s = \int \sigma(\theta,\phi) \sin\theta d\theta d\phi \qquad (1.1)$$

The differential scattering cross section $\sigma(\theta,\phi)$ is quantitative measurement of probability of light being scattered in the direction$(\theta,\phi)$by a scatterer. For a particle of size much smaller than the wavelength of the light the light is scattered almost uniformly (isotropic scattering) in all directions (Rayleigh scattering). For a large particle the light is scattered mostly in the forward direction (anisotropic scattering) within an angle of $1.2\lambda/d$, where λ is the wavelength of the light and d is the diameter of the particle. For particles of intermediate size, $\sigma(\theta,\phi)$ is rapidly changed with scattering angle θ.

The momentum transferred scattering cross-section σ_m is quantitative measurement of the light scattered away from the forward direction and is given by:

$$\sigma_m = \int \sigma(\theta,\phi)(1-\cos\theta)\sin\theta d\theta d\phi \qquad (1.2)$$

The momentum transferred scattering cross-section is often written as: $\sigma_m = (1\text{-}g)\sigma_S$, where g is the anisotropic scattering parameter or mean cosine average of the scattering. In the case of isotropic scattering, $g = 0$. The larger value of g, the light are scattered more anisotropicly.

The transport mean free path is defined as $l_t = 1/n\sigma_m$. Thus, l_t is the mean distance between off angle scattering events, of the mean length of the random walk step of the multiple scattered photons. The transport mean free path is related to the scattering mean free path by:

$$l_t = l_s/(1-g) \qquad (1.3)$$

$l_t = l_S$ in the case of the isotropic scattering. When light are scattered anisotropicly, $l_t > l_S$,and the transport mean free path can be many times of

the mean scattering path. For example, in the case of 625 nm wavelength light scattered by the latex beads sphere (index 1.59) solution in water (index 1.33), $g = 0.06$ and $l_t = 1.07\ l_s$ for beads diameter of 0.09 μm (small particle). For large size particle of diameter 11.9μm, $g = 0.91$ and $l_t = 11\ l_s$. The absorption length is the mean distance of the light travels before it is being absorbed due to inelastic scattering in the medium.

In general, $\sigma(\theta,\phi)$ for particle of arbitrary shape can not be computed. Only for a few kind of particles such as spherical, cylindrical particle $\sigma(\theta,\phi)$ can be obtained theoretically. The formal solution of the problem of light scattering by a homogeneous sphere was worked out by Mie[2] and Debye[3], and it is called Mie theory. The details of Mie theory can be found in many standard electrodynamics and light scattering book.[4-6]

When a laser beam is incident on a slab of random medium, photons are scattered randomly. The transmitted laser beam is split into a ballistic (coherent) and a diffuse (incoherent) component. The ballistic component traverses through the medium in a straight line path and arrives first. Its intensity is attenuated by a factor of $e^{-(w/la + w/ls)}$, where w is the thickness of the slab. The diffuse component consists of multiple scattered photons which undergo random walks inside the medium. The gross properties of the diffuse component can be described by parameters l_t and l_a using the diffusion theory when the medium is sufficiently strong in scattering.

The class of organic molecules which absorb strongly and fluoresce intensely are called Dyes. The basic feature of interest is that dyes are large molecules (with molecular weights ranging from about 175 to 1000) that can absorb light from a wide spectral region and fluoresce in a spectral region involving longer wavelengths. For instance, Rhodamine 590 (molecular weight = 479) in methanol absorbs from the ultraviolet up to about 550 nm

and, depending on concentration and pump source, can lase at a variety of peak wavelengths from roughly 560 to 590 nm with tuning ranges in the 30 nm to 60 nm region.

1.2 Thesis Statement and Organization

In this thesis, the light scattering and absorption, fluorescence image and spectrum, and imaging through model scattering medium and biological tissues are experimentally studied using argon laser light and a fluorescence-absorption technique. The thesis is organized as follows.

In Chapter 2, the effect of the absorption in the random medium on the intensity of the ballistic and diffuse light is studied. The diffusion equation is used to derive the total intensity of the diffuse component of a laser beam transmitted through a slab of random medium. The intensity of the diffuse light is found to be preferentially reduced with respect to the intensity of the ballistic light as the absorption of the medium increases. This observation is because the diffuse light on average travel over a longer distance inside the medium than the ballistic light, so these longer paths diffuse photons will be attenuated more by the absorption. This finding indicates that adding the absorption to the medium can increase the signal (ballistic light) to noise (diffuse light) ratio, thus allowing one to image through an otherwise opaque medium. A simple experiment is performed to illustrate the imaging of an object hidden in a highly scattering random medium by using the fluorescence -absorption technique.

In Chapter 3, we studied the effect of multiple light scattering and self absorption on the fluorescence and excitation spectra of dyes in random media.

DNA fluorescence image histograms are studied in Chapter 4. We

compared the histograms of flow cytometry and quantitative fluorescence image analysis , the latter appears to be a valuable method in cancer cell diagnosis.

In Chapter 5, we summarize the results of this thesis study, and in Chapter 6 we point out some future research directions.

REFERENCES

1. A. Ishimaru, Wave propagation and scattering in random media, Vol. 1 & 2,(Academic Press, New York, 1978).

2. G. Mie, Ann. Physik. 25, 377 (1908).

3. P. Debye, Ann. Physik. 30, 59 (1909).

4. M. Born and E. Wolf, Principles of optics, 4th Edition, (Pergamon, New York,1970), 633-664.

5. H. C. van de Hulst, Light Scattering by Small Particles, (Dover, New York, 1981).

6. J. D. Jaskson, Classical Electrodynamics, 2'nd Edition, (Wiley, New York, 1975).

II. Imaging Objects Hidden In Scattering Media Using a Fluorescence-Absorption Technique

2.1 Introduction

The quality of an image of an object located in or behind a random medium is degraded because of the noise that arises from the multiple light scattering in the medium.[1-12] The degradation of the image quality can become so severe in a highly scattering medium that the object is hidden from view.

Over the years this degradation of image quality has been analyzed by many researchers in the context of the point-spread function and the modulation transfer function[2-12] in various scattering media, such as aerosols,[8] turbulent atmosphere,[11] seawater[11,12] and biomedical[13-14] and turbid media. The light signal traversing through a discrete random medium is split into two components,[2,16,17] a coherent and an incoherent component. The coherent (ballistic) component propagates through the random medium undeviated in the forward direction and carries the image information, whereas the incoherent (diffuse) component undergoes multiple light scattering or a random walk in the random medium and will contribute noise to the image unless its phase is measured. The image may be reconstructed from the incoherent light if the phase and amplitude of the scattered light are known at many points in space. However, the reconstruction of images from incoherent light, known as the inverse scattering problem,[18] remains a difficult experimental and theoretical problem to be overcome for imaging in a turbid medium. Thus various techniques that have been introduced to improve our ability to view through random media have focused on reducing the incoherent light. One such technique is to view the object at a far distance where the multiple scattered light in directions away from the forward direction is reduced. Another technique for viewing through the turbulent atmosphere uses stellar interferometry.[19] Recently ultrafast laser technology

has been used to enhance the image quality by eliminating the multiple scattered light noise.[19-23] Recent time- and angle-resolved studies of ultrafast laser pulse propagation in discrete random media showed that the coherent (ballistic) component can be temporally separated from the incoherent component.[16] The ballistic (coherent) pulse arrives earlier than the diffuse (incoherent) pulse. An image of the object can be obtained by detecting only the ballistic component but rejecting the diffuse component, which can be accomplished by a time-resolved detection technique. There are several time-gating methods that can be used: the ones most commonly known in nonlinear optics are the streak-camera,[20,24] Kerr-gate,[21] two-photon absorption, crosscorrelation techniques [second-harmonic generation(SHG) and parametric frequency generation], and ultrafast time resolution cross-correlation time gating and sensitive lock-in detection technique, in which a hidden object located in turbid random scattering media as much as 28 scattering mean free paths thick can be observed.

In order to enhance the quality of an image of an object hidden in a highly scattering medium, a novel technique that I want to present here is the fluorescence-absorption technique. In this technique, the object is made luminous, and its luminescent light is selected for imaging while the illuminating light is filtered out. The quality of the image can be further improved by selecting the portion of the luminescence spectrum that is strongly absorbed by the random medium.[25]

2.2 Theory

The properties of light scattering in random media can be described by the transport theory.[1] In general, a transport equation is difficult to be solved analytically. Even in most simple cases, the solution of the transport equation

is complicated. When the medium is highly scattering, the transport theory can be approximated by the diffusion theory.[1] Diffusion theory has now been widely used to describe the properties of the multiple scattered (diffuse) light. Analytic solutions of the diffusion equation for various experimental geometries are available and are simple to use.

The intensity in a random medium can be divided into two parts: the reduced incident intensity, I_{ri} and the diffuse intensity, I_d. For a given incident wave, the I_{ri} can be easily calculated. The diffuse intensity, I_d however, must satisfy the equation of transfer:[1]

$$\frac{dI_d(\bar{r},\hat{s})}{ds} = -\rho\sigma_t I_d(\bar{r},\hat{s}) + \frac{\rho\sigma_t}{4\pi}\int_{4\pi} p(\hat{s},\hat{s}')I_d(\bar{r},\hat{s}')d\omega' + \varepsilon_n(\bar{r},\hat{s}) + \varepsilon(\bar{r},\hat{s}) \qquad (2.1)$$

where $\bar{r}$ is a position vector in a random medium, $\hat{s}$ is a unit vector of a given direction, ρ is the number of particles in a unit volume, σ_t is the total cross section, $\hat{s}'$ is the direction of a incident wave, $d\omega'$ is a small solid angle, $p(\hat{s},\hat{s}')$ is the phase function, ε_n is the equivalent source function due to the reduced incident intensity I_{ri}:

$$\varepsilon_n(\bar{r},\hat{s}) = \frac{\rho\sigma_t}{4\pi}\int_{4\pi} p(\hat{s},\hat{s}')I_n(\bar{r},\hat{s}')d\omega' \qquad (2.2)$$

and $\varepsilon(\bar{r},\hat{s})$ is the source function.

In the diffusion approximation we assume that the diffuse intensity encounters many particles and is scattered almost uniformly in all directions, and therefore its angular distribution is almost uniform. The angular dependence cannot be constant, however, because if it were constant, the flux F_d would be zero, and there would be no net power propagation. The diffuse

intensity should therefore have slightly more magnitude in the direction of the net flux flow than in the backward direction. Mathematically we describe this situation by assuming that $I_d(\vec{r},\hat{s})$ is approximated by

$$I_d(\vec{r},\hat{s}) \cong U_d(\vec{r}) + c\mathrm{F_d}\,\hat{s}_f \tag{2.3}$$

where c is a constant, the diffuse flux vector $\mathrm{F_d}$, whose direction is given by a unit vector $\hat{s}_f$, is expressed by

$$\mathrm{F_d} = \int_{4\pi} I_d(\vec{r},\hat{s})\hat{s}\,d\omega = F_d(\vec{r})\hat{s}_f \tag{2.4}$$

and $U_d(\vec{r})$ is the average diffuse intensity,

$$U_d(\vec{r}) = \frac{1}{4\pi}\int_{4\pi} I_d(\vec{r},\hat{s})d\omega \tag{2.5}$$

The constant c in (2.3) can be easily found by noting that

$$F_d(\vec{r}) = \mathrm{F_d}\cdot\hat{s}_f = \int_{4\pi} I_d(\vec{r},\hat{s})\hat{s}\cdot\hat{s}_f d\omega \tag{2.6}$$

Substituting (2.3) into (2.6), we get $c=3/4\pi$, and therefore the diffusion approximation of the diffuse intensity is given by

$$I_d(\vec{r},\hat{s}) = U_d(\vec{r}) + (3/4\pi)F_d(\vec{r})\cdot\hat{s} \tag{2.7}$$

Equation (2.7) may be regarded as the first two terms of a Taylor's expansion of I_d in terms of the powers of $\hat{s}\cdot\hat{s}_f$, and therefore the second term of (2.7)

must be considerably smaller than the first: $U_d >> |F_d|$.

We now proceed to derive a diffusion equation based on the approximation (2.7). First, we integrate (2.1) over all 4π of solid angle and obtain a general power relationship

$$divF_d(\vec{r}) = -4\pi\rho\sigma_a U_d(\vec{r}) + 4\pi\rho\sigma_s U_n + E(\vec{r}) \tag{2.8}$$

where $U_n(\vec{r}) = (1/4\pi)\int_{4\pi} I_n(\vec{r},\hat{s})d\omega$ and $E(\vec{r}) = \int_{4\pi} \epsilon(\vec{r},\hat{s})d\omega$. Next, we substitute (2.7) into (2.1). Under the assumption that the phase function $p(\hat{s},\hat{s}')$ is a function of the angle between $\hat{s}$ and $\hat{s}'$. we obtain

$$\hat{s}\cdot gradU_d + \frac{3}{4\pi}\hat{s}\cdot grad(F_d\cdot\hat{s}) = -\rho\sigma_t U_d - \frac{3}{4\pi}\rho\sigma_t F_d\cdot\hat{s} + \rho\sigma_s U_d + \frac{3}{4\pi}\rho\sigma_t F_d\cdot\hat{s}p_1 + \epsilon_n + \epsilon \tag{2.9}$$

where ε is defined in (2.1), and p_1 is given by

$$p_1 = \frac{1}{4\pi}\int_{4\pi} p(\hat{s},\hat{s}')\hat{s}\cdot\hat{s}'d\omega' \tag{2.10}$$

and it represents the averaged forward scattering $(\hat{s}\cdot\hat{s}'>0)$ minus the backward scattering $(\hat{s}\cdot\hat{s}'<0)$ of a single particle.

It is often convenient to write $p_1 = W_0\bar{\mu}$ where W_0 is the albedo of a single particle and $\bar{\mu}$ is the mean cosine of the scattering angle θ given by

$$\bar{\mu} = \left(\int_{4\pi} p(\hat{s},\hat{s}')\mu d\omega'\right) \Big/ \left(\int_{4\pi} p(\hat{s},\hat{s}')d\omega'\right) \tag{2.11}$$

where $\mu = \cos\theta = \hat{s}\cdot\hat{s}'$. We note that since the phase function $p(\hat{s},\hat{s}')$ is a function of the scattering angle γ only, we can expand the phase function in a

series of Legendre functions:

$$p(\hat{s},\hat{s}') = \sum_{n=0}^{\infty} W_n P_n(\cos\gamma), \qquad \cos\gamma = \hat{s}\cdot\hat{s}' \tag{2.12a}$$

and p_1 is given by

$$p_1 = W_1/3, \qquad \bar{\mu} = p_1/\ W_0 = W_1/\ 3W_0 \tag{2.12b}$$

The phase function can often be approximated by the following form involving only W_0 and $\bar{\mu}$:

$$p(\mu) = W_0(1-\bar{\mu}^2)[1+\bar{\mu}^2 - 2\bar{\mu}\mu]^{-3/2} \tag{2.12c}$$

This is called the Henyey-Greenstein formula.

Now we multiply (2.9) by $\hat{s}$ and integrate over all 4π, and obtain

$$gradU_d = -\frac{3}{4\pi}\rho\sigma_t(1-p_1)F_d + \frac{3}{4\pi}\int_{4\pi} \varepsilon_n(\bar{r},\hat{s})\hat{s}d\omega + \frac{3}{4\pi}\int_{4\pi} \epsilon(\bar{r},\hat{s})\hat{s}d\omega \tag{2.13}$$

The quantity $\sigma_t(1-p_1)$ is called the transport cross section σ_{tr}. It indicates that if the scattering is anisotropic, the equivalent total cross section is reduced by the factor $1-p_1$ from the isotropic case. The transport cross section is also written as

$$\sigma_{tr} = \sigma_t(1-p_1) = \sigma_s(1-\bar{\mu}) + \sigma_a \tag{2.14}$$

As indicated in the approximate representation of $\rho\sigma_s = H(1-H)\sigma_t / V_e$, where ρ is the number density, V_e the volume of a single erythrocyte, H the hematocrit, $\rho\sigma_s$ the absorption coefficient, if the particle density is increased, the equivalent scattering cross section is decreased by the factor 1-H where H is the ratio of the volume occupied by scatterers to the total volume. In terms of the number density ρ and the volume V_e of a single scatterer, H is equal to ρV_e :

$$\sigma_t \to \sigma_t(1-H) \tag{2.15a}$$

The transport cross section σ_{tr} for a high density medium should then be given by

$$\sigma_{tr} \to \sigma_t(1-H)(1-\bar{\mu}) + \sigma_a \tag{2.15b}$$

Equation (2.8) gives div F_d in terms of U_d and (2.13) gives grad U_d in terms of F_d. We eliminate F_d from these two equations by taking F_d from (2.13), substituting it into (2.8), and obtain a differential equation for U_d:

$$\begin{aligned}\nabla^2 U_d(\bar{r}) - \kappa_d^2 U_d(\bar{r}) &= -3\rho\sigma_s\rho\sigma_{tr}U_n(\bar{r}) - \frac{3}{4\pi}\rho\sigma_{tr}E(\bar{r}) \\ &+ \frac{3}{4\pi}\nabla\cdot\int_{4\pi}\varepsilon_n(\bar{r},\hat{s})\hat{s}d\omega + \frac{3}{4\pi}\nabla\cdot\int_{4\pi}\varepsilon(\bar{r},\hat{s})\hat{s}d\omega\end{aligned} \tag{2.16}$$

where $\kappa^2 = 3\rho\sigma_s\rho\sigma_{tr}$. It is understood that for a high density medium, σ_t and σ_{tr} in (2.16) should be given by (2.15a) and (2.15b). Equation (2.16) is the fundamental steady state diffusion equation for the average diffuse intensity

$U_d(\bar{r})$, and together with the boundary condition, constitutes the complete mathematical description of the diffusion approximation. Once the diffusion intensity is found, the flux F_d can be calculated from (2.13).

The case of a plane wave incident upon a slab containing random particles can be analyzed by the following equation:

$$\frac{\partial^2}{\partial z^2}U_d(z) - \kappa_d^2 U_d(z) = -Q_0 \exp(-\rho\sigma_t z) \tag{2.17}$$

where $Q_0 = [3\rho\sigma_s\rho\sigma_{tr} + 3\rho\sigma_s\rho\sigma_t\bar{\mu}](F_0/4\pi)$, and F_0 is the flux density. The boundary conditions are:

$$\begin{aligned} U_d(z) - h\frac{\partial}{\partial z}U_d(z) + \frac{Q_1(z)}{2\pi} = 0 \quad &\text{at} \quad z = 0 \\ U_d(z) + h\frac{\partial}{\partial z}U_d(z) - \frac{Q_1(z)}{2\pi} = 0 \quad &\text{at} \quad z = d \end{aligned} \tag{2.18}$$

where $Q_1(z) = (\sigma_s\bar{\mu}/\sigma_{tr})F_0 \exp(-\rho\sigma_t z)$ and $h = 2/3\rho\sigma_{tr}$. The general solution of (2.17) is the sum of a particular solution U_{dp} and a complementary solution U_{dc}. To find a particular solution, we let

$$U_{dp}(z) = A\exp(-\rho\sigma_t z) \tag{2.19}$$

Substituting (2.19) into (2.17), we obtain

$$A = -Q_0/[(\rho\sigma_t)^2 - \kappa_d^2] \tag{2.20}$$

The complementary solution U_{dc} satisfies

$$\frac{\partial^2}{\partial z^2}U_{dc} - \kappa_d^2 U_{dc} = 0 \tag{2.21}$$

and therefore we have

$$U_{dc}(z) = C_1 \exp(\kappa_d z) + C_2 \exp(-\kappa_d z) \tag{2.22}$$

C_1 and C_2 are unknown constants and are determined by applying the boundary conditions (2.18). Substituting $U_d(z) = U_{dp}(z) + U_{dc}(z)$ into (2.18) we get two equations for the two unknowns C_1 and C_2:

$$\begin{aligned} &C_1(1-\kappa_d h) + C_2(1+\kappa_d h) = -A(1+\rho\sigma_t h) - \frac{Q_1(0)}{2\pi} \\ &C_1(1+\kappa_d h)\exp(\kappa_d d) + C_2(1-\kappa_d h)\exp(-\kappa_d d) \\ &= -A(1-\rho\sigma_t h)\exp(-\rho\sigma_t d) + \frac{Q_1(0)}{2\pi}\exp(-\rho\sigma_t d) \end{aligned} \tag{2.23}$$

From these, we can easily determine C_1 and C_2.

It can be shown that for the case of a semi-infinite medium ($d \to \infty$), we have

$$C_1 \to 0, \qquad C_2 \to -\frac{A(1+\rho\sigma_t h)}{(1+\kappa_d h)} - \frac{Q_1}{2\pi(1+\kappa_d h)}$$

$$U_d(z) = A\exp(-\rho\sigma_t z) + C_2 \exp(-\kappa_d z) \tag{2.24}$$

The flux $F_s(z)$ can be calculated from

$$F_s(\bar{r}) = \frac{\sigma_s \bar{\mu} F_0(\rho)}{\sigma_{tr}} \exp(-\rho\sigma_t z)\hat{z} - \frac{4\pi}{3\rho\sigma_{tr}} grad U_s(\bar{r}) \qquad (2.25)$$

2.3 Experimental Method

An object in a medium can be observed by illuminating it with a beam of light. The image of the object can be reconstructed either from the shadow of the object (transillumination) or from the signal light backscattered from the object in the backscatter configuration. As the illuminating light traverses deeper into the random scattering medium, its signal intensity decreases while the multiple scattered light intensity increases. The signal light contains the image information of the object, while the multiple scattered light contributes noise to the image unless its phase is known. When the light traverses beyond a certain thickness, the object may not be observed because the signal intensity is reduced below the noise level.

A novel way to reduce the amount of noise from the multiple scattered light is to shorten the distance the signal light has to travel in the random medium. The total distance that the signal light transverses in the medium is the thickness of the medium in the transillumination approach, whereas the distance the signal light travels is twice the depth of the object in the backscattered light viewing direction. A shorter signal distance for the signal light can be accomplished if the object is made luminous and then viewed from luminescent light. The distance that the luminescent signal light traverses is from the object to the exit point of the random medium, which is shorter than the distance the illuminating signal light had to traverse in the

transillumination technique. Hence, viewing the object in the luminescence spectral range, while filtering out the illuminating light, can result in better image quality in both the transillumination and backscattered configurations.

The quality of the image obtained from a luminous object in this fashion can be further improved by introducing an absorbing dye into the random medium that preferentially absorbs the luminescent light. The underlying physical principle is that the multiple scattered light on the average travels over a longer path length than the ballistic signal. The mean distance that the multiple scattered light travels in the random medium is z^2/l_t, which is longer than z, the distance the ballistic light transverses through a thickness z, where l_t is the photon transport mean free path. Consequently the multiple scattered light, which travels over a longer path length, is attenuated more than the signal light by absorption. The image quality of an object should be improved when it is viewed in the overlapping spectral region between the luminescence spectrum of the object and the absorption spectrum of the surrounding medium. Figure 2.1 shows a schematic diagram for the imaging setup that illustrates the imaging technique described above. A U-shaped glass tube of 1-mm bore as an object was placed in a glass cell containing water with a 25-mm thickness. The U-shaped object was filled with Rhodamine 640 dye dissolved in ethylene glycol and sealed. This object was illuminated by an argon laser at 488 nm,
and it fluoresced in the 580-640-nm spectral range. The image of the object was detected by a charge-coupled-device (CCD)camera and recorded by a personal computer.

2.4 Results and Discussion

Figure 2.2 (a) shows a clear U-shaped image taken by the CCD camera when the object was submerged in clear water. The object was positioned inside the medium at 10 mm from the back surface of the glass cell, and the CCD camera was placed in the transmission-mode geometry. Latex beads of 0.46-um diameter were then added to the water, which created a random scattering medium. As the concentration of the latex beads increased, the image became blurred and disappeared as shown in Fig. 2.2(b), where the bead concentration is 10×10^{16} m^{-3}. The blurred image demonstrates that transillumination fails to image the object in this scattering medium even though the object (Rhodamine 640) strongly absorbed the incident beam (the argon laser at 488 nm). The U-shaped object becomes recognizable, as shown in Fig. 2.2(c), when the illuminating laser light is filtered out but the luminescence light is allowed to pass to the CCD. Corning 1-67 and long-pass 560-nm filters were used and placed in front of the CCD camera to remove the argon laser light and allow luminescence light above 570 nm to pass through.

The quality of the image was further improved by the addition of an absorbing dye into the random medium that preferentially absorbs the Rhodamine 640 fluorescence. Malachite Green dye was selected for this purpose and was added to the random scattering medium. The image obtained under these conditions is shown in Fig.2.2(d), which shows a better image quality compared with that of Fig.2.2(c). The absorption length of the scattering medium for Fig.2.2(d) was measured to be 1.8 mm at 615 nm. The addition of more Malachite Green further improved the images. The contrast of images shown in Fig.2.2 is best illustrated by a plot of the spatial intensity

distribution along a horizontal line across the image. The corresponding digitized intensity plots for the images of Fig.2.2 are shown in Fig.2.3. The two peaks shown in Fig.2.3(a) correspond to the emitted light across the two legs of the U-shaped object. Figure 2.3(e) shows the best image contrast in which the absorption is strongest (l_a=0.9 mm).

The image of the object was also studied in the backscattered geometry. The image quality is shown to improve when the fluorescence technique was used. The random medium used consisted of latex beads at a concentration of 8.1 x 10^{15} m^{-3} suspended in water. The U-shaped object was placed 10 mm from the front surface. Figure 2.4(a) shows that the object is not recognizable when there was no filter to remove the scattered illuminating light from the CCD camera.[26] The CCD camera detected the multiple backscattered noise of the illuminating light, which is more intense than that in the transmission geometry. When this multiple scattered light was removed by placing a filter (long-pass 560 nm) in front of the CCD, a slightly recognizable U-shaped image was observed, as shown in Fig.2.4(b). When absorption is introduced into the random medium, the quality of the image improves, as shown in Fig.2.4(c), where the absorption length is 0.5 mm at 615.

2.5 Conclusion

We have demonstrated that the fluorescence technique is better than the conventional transillumination technique to image an object hidden in a scattering medium. The quality of the image can be further improved when the surrounding random scattering medium preferentially absorbs in the spectral range of the fluorescence light. These results indicate that absorption and fluorescence diaphanography (transillumination) with the use of chromophores and fluorophores (dyes) may be a feasible modality to obtain

high-quality images of a small hidden object on the millimeter scale.

REFERENCES

1. A. Ishimaru, Wave propagation and scattering in random media, Vol. 1& 2, (Academic Press, New York, 1978).
2. A.Ishimaru, Appl.Opt.17,348(1978).
3. A.Ishimaru,Y.Kuga, R.L.T.Cheung, and K.Shimizu, J.Opt. Soc.Am.73,131(1983).
4. Y.Kuga and A.Ishimaru, J.Opt.Soc. Am. A2,2330(1985).
5. R.E.Hufnagel and N.R.Stanley, J.Opt.Soc.Am.54,52(1964).
6. N.S.Kopeika, J.Opt.Soc.Am.72,548(1982).
7. N.S.Kopeika, J.Opt.Soc.Am.72,1092(1982).
8. A.Zardecki, S.A.W.Gertl, and J.F.Embury, Appl.Opt.23,4142(1984).
9. W.G.Tam and A.Zardecki, Int.J.Infrared Millimeter Waves 6,249(1985).
10. R.F.Lutomirski and H.T.Yura, J.Opt.Soc.Am.61,482(1971).
11. W.Wells,J.Opt.Soc.Am.59,686(1969).
12. H.T.Yura, Appl.Opt.12,1061(1973).
13. R.Lafrenuere, F.S.Ashkar,and A.S.Ketcham, Am.Surg.52,123(1986).
14. E.A.Sickles, Recent Results Cancer Res.105,31(1987).
15. D.S.Dilworth, E.N.Leith, and J.L.Lopez, Appl.Opt.29,691(1990).
16. K.M.Yoo and R.R.Alfano, Opt.Lett.15,320(1990).
17. F.Liu, K.M.Yoo, and R.R.Alfano, Opt.Lett.16,351,(1991).

18. H.P.Baltes,ed., Inverse Source Problems in Optics (Springer-Verlag, Berlin,1978).

19.J.C.Dainty,ed.,Laser Speckleand Related Phenomena (SpringerVerlag,Berlin,1975),pp.203-278.

20. P.P.Ho,P.Baldeck,K.S.Wong,K.M.Yoo,D.Lee, and R.R.Alfano, Appl.Opt.28,2304(1989).

21.L.M.Wang,Y.Liu,P.P.Ho, and R.R.Alfano,"Ballistic imaging of biomedical samples using picosecond optical Kerr gate," in Proceedings of OE LASER'91: Symposium on Biomedical Optics (Society of Photo-Optical Instrumentation Engineers, Bellingham, Wash.).

22. S.Andersson-Engels, R.Berg, S.Svanberg, and O.Jarlman Opt.Lett.15,1179(1990).

23. H.Chen,Y.Chen,D.Dilworth,E.Leith,J.Lopez, and J.Valdmanis, Opt.Lett.16,487 (1991).

24. J.C.Hebden,R.A.Kruger, and K.S.Wong, Appl.Opt.30,788(1991).

25. K.M. Yoo, F. Liu, Z.W. Zang, S.A. Ahmed, and R.R. Alfano, SPIE, Vol.1599, Recent Advances in the Use of Light in Physics, Chemistry, Engineering and Medicine 323/1991.

26. R.A.Wick,Appl.Opt.26.3210 (1987).

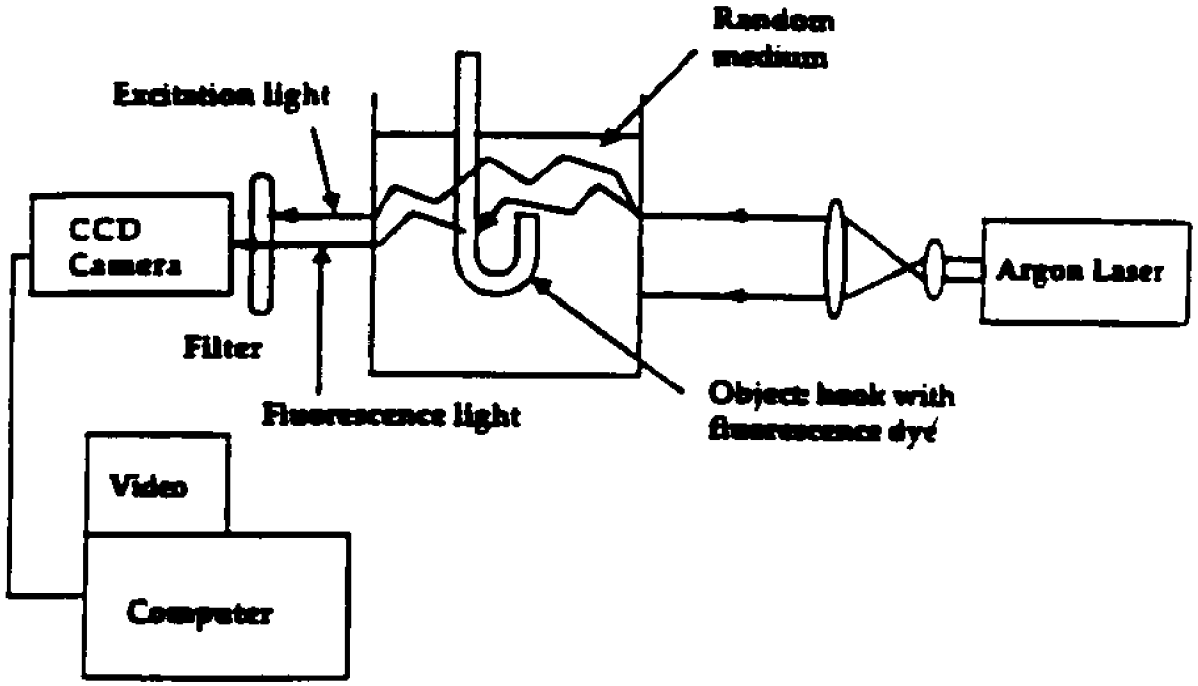

Fig. 2.1 Schematic diagram of the imaging setup.

Fig. 2.2 Images of an object placed in different media(a) Water. (b) A random medium consisting of latex beads of 0.46 μm diameter with a latex concentration of $10\times10^{16}m^{-3}$; both the illuminating and fluorescence light are allowed into the CCD camera. (c) The same as in (b) except that the illuminating light is filtered out. (d) The same as in (c) except that the medium is made absorbing by introducing absorbing dye (malachite Green) into the medium: the absorption length is 1.8 mm. (e) The same as in (d) except that the medium is made more absorbing; theabsorption length is 0.9 mm. The thickness of the medium is 25 mm. and the images are obtained in the transmission geometry.

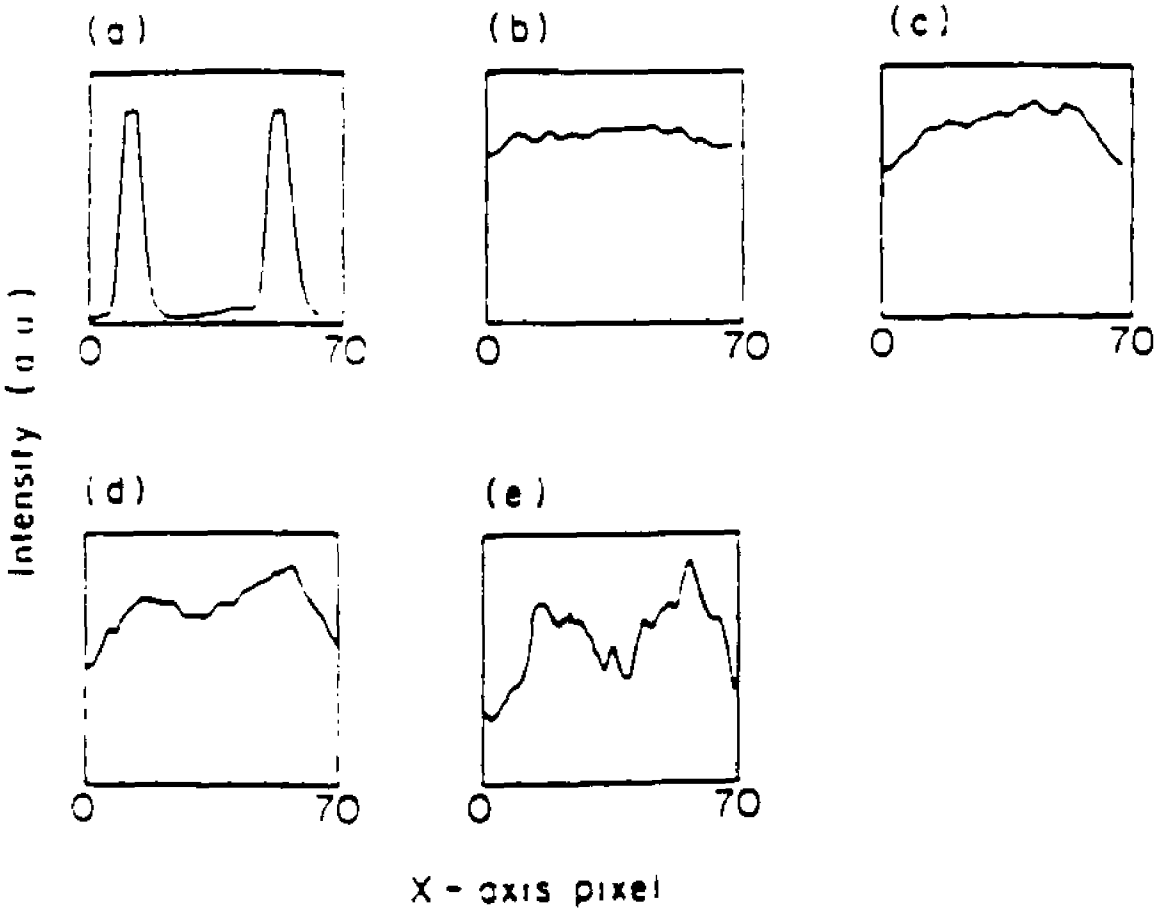

Fig. 2.3 Corresponding plots of light intensity across a line in the middle of the images in Fig. 2.2. The scale is 0.17 mm/pixel.

Fig. 2.4 Images of an object placed 10 mm from the front surface of the random medium under three conditions: (a) both the illuminating and fluorescence light are allowed to pass into the CCD, (b) the illuminating light is filtered out, (c) the same as in (b) but the medium is made absorbing with $l_a = 0.5$ mm. The bead concentration is $8.1\times10^{15}\,m^{-3}$. The CCD is placed in the backscattered geometry.

III. Effect of multiple light scattering and self absorption on the fluorescence and excitation spectra of dyes in random media

3.1 Introduction

The fluorescence of objects embedded in absorptive random scattering media has recently been studied and shown to enhance the detection and imaging of such objects. The use of fluorescence imaging techniques of this type has potential application in medical diagnostic techniques.[1] In these imaging techniques, the object to be detected, which has or is made to have fluorescent properties (e.g. by dye injection) is illuminated and made to fluoresce. This luminescence light is then selected for detection and imaging, while the illuminating light is filtered out. The image quality is further improved when the surrounding scattering medium is made partially absorbing at the luminescence spectrum. Since the luminescent object to be detected in a typical medical application,[1-5] such as a breast tumor is itself constituted from a highly scattering medium, the effects of scatter on the emitted luminescence spectra itself is of interest to the further development of these techniques. This is of particular importance since the distribution of the luminescent spectrum itself may relate to medical conditions to be diagnosed. This thesis presents the results of experiments to examine the impact of internal multiple scattering within a luminescent body on the luminescence spectrum observed at the surface. The intrinsic emission spectrum of a luminescent medium, such as an organic dye luminifor is typically Stokes shifted with respect to its absorption spectrum. The presence of internal multiple scatterers within a luminescent body can affect the luminescence observed at the surface of the body in three ways. These are:

(1) Self Absorption.

The luminescence light emitted from inside a random medium will reach the surface by a "random walk" diffusion process. The mean random path length of the luminescence light before it reaches the surface depends on the

depth of the luminifor inside the body and the photon transport mean free path in the random medium. The deeper the luminifor and the higher the density of scatterers, the longer is the photon path length. Because the emission spectrum of a luminifor overlaps its absorption spectrum, emitted fluorescent light experiences greater absorption at shorter wavelengths as it propagates through a luminescent medium in solution to the surface. This preferential absorption at the shorter wavelengths would mean that the emission finally emerging at the surface of a body would show a spectrum relatively diminished at the shorter wavelength end, as compared to the intrinsic fluorescence of the luminorous, i.e. the fluorescence spectrum observed at the surface would effectively appear to be red shifted toward the longer wavelengths. Clearly, the greater the depth within the body from which the radiation originates, and/or the greater the scatterer density, the greater would be this "red" shift.

(2) Wavelength Dependence of Scattering.

Elastic (Rayleigh) scattering by random particulate scatterers will scatter the shorter wavelengths preferentially. This will mean that luminescence light emitted from inside the body at shorter wavelengths will undergo more scattering than that at longer wavelengths in reaching the surface. Thus the shorter wavelength light effectively undergoes a longer random walk path and experiences more absorption, and hence the remaining luminescence spectrum will be effectively red shifted when emerging from the surface. This wavelength dependence can be observed in random media with small scatterer of diameter less than the wavelength of light. This wavelength dependence may be different in tissues. There the scatterers are generally much larger than the optical wavelength, however, it can still generally be expected that the larger wavelengths will less scattered and hence penetrate

deeper.

(3) Energy Level Distortions.

At sufficiently high concentrations, scatterer densities might conceivably be sufficient high so that interatomic forces cause distortion effects on energy levels of luminofors, with consequent impacts on their intrinsic fluorescence emission spectra. The coherent interference between the radiated field of a dye molecule and the field radiated from an effective Hertzian dipole induced on the closest scatterers may also conceivably affect the emissions spectrum.[6] This effect has been observed when there exists more than one scatterer within a unit wavelength. Such effects, if they exist, would be dependent on the density of scatterers, like the two previous effects, (1) and (2). However, unlike the latter these they might just as well cause a "blue" shift as a "red" shift. Furthermore their effects would not be dependent on the depth of the emitting body within the random medium, as are (1) and (2).[7]

3.2 Theory

When molecules are illuminated by monochromatic radiation with a wavelength within their resonance absorption band, a portion of the radiation is absorbed (resonance absorption). Some of the absorbed radiation will be re-emitted as fluorescence radiation by the molecules over a broad spectral range characteristic of the specific molecular species. In that process, each excited molecule decays by isotropically reemitting a photon spontaneously. This fluorescence radiation will be in all directions.

3.2.1 The Franck Condon principle

Although quantum mechanics imposes no restrictions on the change in the vibrational quantum number during an electronic transition,[8-10] the vibrational

lines in a progression are not all observed to be of the same intensity. In some spectra the (0,0) transition is the strongest, in others the intensity increases to a maximum at some value of v', while in yet others only a few vibrational lines with high v', are seen, follow by a continuum. all these types of spectra are readily explicable in terms of the Franck-Condon principle which states that an electronic transition takes place so rapidly that a vibrating molecule does not change its internuclear distance appreciably during transition.

Classical theory would suggest that the oscillating atom would spend most of its time on the curve at the turning point of its motion, since it is moving most slowly there; quantum theory, while agreeing with this view for high values of the vibrational quantum numbers, shows that for $v = 0$ the atom is most likely to be found at the center of its motion, at the equilibrium internuclear distance r_{eq}. For $v = 1, 2, 3, \ldots$ the most probable positions steadily approach the extremities until, for high v, the quantal and classical pictures merge. This behavior is shown in Fig. 3.1 where we plot the probability distribution in each vibrational state against internuclear distance. Fig. 3.1 shows the variation of Ψ_2 with internuclear distance, where Ψ is the vibrational wave function. Fig. 3.2 shows three possibilities. In (a) we show the upper electronic state having the same equilibrium internuclear distance as the lower. Now the Frank-Condon principle suggests that a transition occurs vertically on this diagram, since the internuclear distance does not change, and so if we consider the molecule to be initially in the ground state both electronically (ε'') and vibrationally ($v'' = 0$), then the most probable transition is that of indicated by the vertical line in Fig. 3.2(a). Thus the strongest spectral line of the $v'' = 0$ progression will be the (0,0). However, the quantum theory only says that the probability of finding the oscillating atom is greatest at the equilibrium distance in the $v = 0$ state, it allows some, although small,

chance of the atom being near the extremities of its vibrational motion. Hence there is chance of the transition starting from the ends of the $v''=0$ state and finishing in the $v=1,2$, etc., states. The (1,0), (2,0), etc. lines diminish rapidly in intensity, however, as shown at the foot of Fig. 3.2(a).

In Fig. 3.2(b) we show the case where the excited electronic state has a slightly greater internuclear separation than the ground state. Now a vertical transition from the $v''=0$ level will most likely occur into the upper vibrational state $v=2$, transition to lower and higher v states being less likely; in general the upper state most probably reached will depend on the difference between the equilibrium separations in the lower and upper state. In Fig. 3.2(c) the upper state separation is drown as considerably greater than that in the lower state and we see that, firstly, the vibrational level to which a transition takes place has a high v value. Further, transitions can now occur to a state where the excited molecule has energy in excess of its own dissociation energy. From such states the molecule will dissociate without any vibrations and, since the atoms which are formed may take up any value of kinetic energy, the transitions are not quantized and a continuum results. This is shown at the foot of the figure.

3.2.2 Vibronic absorption transitions

The total energy (E_t) of a molecule in its electronic ground state (excluding translational energy, and internal nuclear energy),[11]

$$E_t = E_e + E_v + E_r \tag{3.1}$$

is the sum of three components, the electronic energy (E_e), the vibrational energy (E_v), and the rotational energy (E_r). Similarly, the total energy (E'_t) of

a molecule in an excited electronic state

$$E'_t = E'_e + E'_v + E'_r \tag{3.2}$$

is the sum of its electronic, vibrational and rotational components, E'_e, E'_v, and E'_r, respectively. If we define an absorption transition as

$$\Delta E_x = E'_x - E_x \tag{3.3}$$

where x = t, e, v, or r, then $\Delta E_x \sim 10cm^{-1}, \Delta E_v \sim 1000cm^{-1}$, and $\Delta E_e \sim 30,000cm^{-1}$.

Transitions involving only $\Delta E_r (\Delta E_e = \Delta E_v)$ yield the rotational absorption spectrum, which occurs in the far infrared region. Translations involving ΔE_v and $\Delta E_r (\Delta E_e = 0)$ yield the vibrational and vibrational- rotational absorption spectrum, which occurs in the near infra-red region. Transitions involving ΔE_e and ΔE_v yield the electronic and electronic-vibrational absorption spectrum, which occurs in the visible and ultraviolet region. A state involving electronic and vibrational energy is referred to as a vibronic state, and a transition between two such states is a vibronic transition . Each electronic absorption transition ΔE_e gives rise to an absorption band system, each band of which corresponds to a different value of ΔE_v.

Let us consider a molecule in which only one vibrational mode is dominant, so that it approximates to a harmonic oscillator. If the energy of the fundamental vibrational mode in the ground electronic state is E_{1v}, then

$$E_t = E_e + (m + \tfrac{1}{2})E_{1v} \tag{3.4}$$

where m=0, 1, 2, ...is the vibrational quantum number. If the energy of the

fundamental vibrational mode in the excited electronic state is E'_{vv}, then

$$E'_t = E'_e + (n+\tfrac{1}{2})E'_{vv} \tag{3.5}$$

where n=0, 1, 2, 3, ...If the ground state system is thermal equilibrium at absolute temperature T, the fraction f_m of ground state molecules in a vibrationally excited state m is determined by the Boltzmann factor,

$$f_m = \exp(-mE_{1v} / KT) \tag{3.6}$$

where K is Boltzmann's constant. Since $E_{1v} = 1000cm^{-1}$, and $KT = 200cm^{-1}$ at room temperature, $f_1 = e^{-5} = 6.7\times10^{-3}, f_2 = e^{-10}$,etc., over 0.99 of the molecules are in the zero-point vibrational level of energy

$$E_t = E_e + \tfrac{1}{2}E_{1v} \tag{3.7}$$

The transitions constituting the main electronic absorption spectrum are given by

$$\Delta E_t = (E'_e - E_e) + \tfrac{1}{2}(E'_{vv} - E_{1v}) + nE'_{vv} = (E'_e - E_e) + nE'_{vv} \tag{3.8}$$

since $E'_{vv} = E_{1v}$. The lowest energy vibronic transition in a given band system (n=0) is described as the 0-0 transition. The transition to the n^{th} vibrational level of E'_t is the 0-n vibronic transition. The main electronic absorption spectrum thus yields data about the vibrational levels (nE'_{vv}) of the excited electronic states Fig. 3.3.

3.2.3 Vibronic fluorescence transitions

Luminescence is the emission of photons from electronically excited states. Luminescence is divided into two types, depending upon the nature of the ground and the excited states.[11] In a singlet excited state, the electron in the higher-energy orbital has the opposite spin orientation as the second electron in the lower orbital. Theses two electrons are said to be paired. In the triplet states these electrons are unpaired, that is, their spins have the same orientation. Return to the ground state from an excited singlet state does not require an electron to change its spin orientation. A change in spin orientation is needed for a triplet state to return to the singlet ground state. Fluorescence is the emission which results from the return to the lower orbital of the paired electron. Such transitions are quantum mechanically "allowed" and the emissive rates are typically near 10^8 sec^{-1}. These high emissive rates result in fluorescence lifetimes near 10^{-8} sec or 10 nsec. The lifetime is the average period of time a fluorophore remains in the excited state.

The $S_1 - S_0$ fluorescence transition is the inverse of $S_0 - S_1$ absorption transition. Provided the lifetime of the excited electronic singlet state S_1 is sufficiently long for the excited molecules to attain thermal equilibrium, the fluorescence emission occurs primarily from the Zero-point vibrational level of S_1. This condition is generally valid if the molecules are in a condensed medium, in solution, but it may not be true in a rarefied vapor, in which the molecules cannot lose their excess vibrational energy in collisions. In solution the fluorescence spectrum corresponds to $10 \rightarrow 0$ m vibronic transitions to the various vibrational levels (m) of the ground electronic singlet state (S_0). The fluorescence spectrum thus yields data about the vibrational levels of the ground electronic state Fig. 3.3.

We define the molecular fluorescence quantum efficiency q_{fm} as the ratio

of the number of fluorescence photons emitted by a system of molecules in dilute solution to the number of molecules excited into S_1 (the number of absorbed photons). The molecular fluorescence quantum intensity at frequency ν, normalized by the relation,[13]

$$q_{fm} = \int_0^{\infty} F(\nu) d\nu \tag{3.9}$$

In the general case of a large dye molecule, many normal vibrations of differing frequencies are coupled to the electronic transition. Further more, collisional and electrostatic perturbations, caused by the surrounding solvent molecules broaden the individual lines of such vibronic sublevel of every electronic state, including the ground state, has superimposed on it a ladder of rotationally excited sublevels. These are extremely broadened because of the frequent collisions with solvent molecules which hinder the rotational movement so that there is a quasicontinuum of states superimposed on every electronic level. The population of these levels in contact with thermalized solvent molecules is determined by a Boltzmann distribution.

After an electronic transition, which, as describe above, lead to a nonequilibrium state (Franck-Condon state) the approach to thermal equilibrium is very fast in liquid solutions at room temperature. The reason is that a large molecule experiences at least 10^{12} collision/sec with solvent molecules, so that equilibrium is reached in a time of the order of one picosecond. Thus, the absorption is practically continuous all over the absorption band. The same is true for the fluorescence emission corresponding to the transition from the electronically excited state of molecule to the ground state. This results in a mirror image of the absorption band displaced towards lower wave number by reflection at the wave number

of the purely electronic transition. This condition exists, since the emissive transitions start from vibrational ground state of the first excited electronic state S_1 and end in vibrationally excited sublevels of the electronic ground state. The resulting typical form of the absorption and fluorescence spectrum of an organic dye is given in Fig. 3.4.

3.2.4 Emission spectra

The uptake of ultraviolet or visible radiation by a molecule results in the formation of an excited state or state of high energy. Such energy rich states are relatively short lived and rapidly lose the absorbed energy to return to the stable ground state. There are types of intermolecular process whereby molecules can lose excess energy. One is classified as radiative since energy is lost by the emission of radiation, and the other as non-radiative since radiation is not emitted during energy loss. The former process is of importance in the present context since it gives rise to emission spectra.

The radiation emitted during a radiative transition is termed fluorescence when the transition is between states of the same multiplicity
and phosphorescence when the transition is between states of different multiplicity. That is, the emitted radiation is fluorescence for the $S_1 \rightarrow S_0$ transition and phosphorescence for the $T_1 \rightarrow S_0$ transition. The relationship between the absorption spectrum of a molecule with a singlet ground state
and its fluorescence and phosphorescence spectra is seen in Fig. 3.5. On absorption of radiation the molecule may be excited to an upper vibrational level of first excited singlet state or end up in such a level after deactivation from an upper excited singlet state. The excess vibrational energy is rapidly lost by collisional deactivation and the molecule finishes up in the vibrational level.

Fluorescence arises from the radiative transitions from the lowest vibrational level of the S_1 state to the various vibrational levels of the S_0 state. If the spacings of the vibrational levels in the excited state are similar to those in the ground state there will be an approximate "mirror image" relationship between the absorption and fluorescence spectra. The spacing between the bands in the absorption spectrum is equal to the difference in energy between the bands in the fluorescence spectrum is equal to the difference in energy between the vibrational levels of the ground state. Although the $0 \rightarrow 0$ transitions in absorption and fluorescence are shown to have the same energy in Fig. 3.5. this may not in fact be the case, and in the absorption and fluorescence spectra the band arising from the $0 \rightarrow 0$ may be slightly displaced. Consideration of Fig. 3.5. helps to explain why this can occur.

If the excited state S_1 has a different solvation equilibrium from the ground state S_0 there will be a reorientation of the solvent cage after excitation and the more stable equilibrium state of S_1 will be formed. Fluorescence emission from this latter state will give a non-equilibrium ground state of higher energy than the original equilibrium ground state. Thus the $0 \rightarrow 0$ fluorescence transition will be of lower energy (lower wave number) than original $0 \rightarrow 0$ absorption transition. Phosphorescence results from the radiative transition of the lowest vibrational level of the T_1 state to the various vibrational levels of the S_0 state. Since the energy of the T_1 state is lower than that of the S_1 state the phosphorescence spectrum is observed at lower wave number values than the fluorescence spectrum. Since transitions between states of different multiplicity are forbidden the phosphorescence spectrum is weak. On the other hand, fluorescence is relatively intense since it corresponds to a transition between states of the same multiplicity.

The intensities of vibrational bands in fluorescence and phosphorescence

spectra vary in a similar manner to bands in absorption spectra. Again this is most readily discussed in relation to diatomic molecules. Typical potential energy curves for the S_0 and S_1 state of a diatomic molecule are show in Fig.3.6. Here the excited state curve is displaced to greater internuclear separation than the ground state curve. The Franck-Condon principle applies to emission as well as to absorption, and emission processes can be represented by vertical lines connecting the initial and final states. In the situation represented in Fig. 3.7 the $0 \rightarrow 1$ transition is the most probable and the fluorescence spectrum may appear as shown.

3.3 Experimental method

To investigate the impact of multiple light scattering in a luminescent random media on the emitted spectra, experiments were carried out on organic dye luminofors dissolved in liquid solvents, with TiO_2 particles added to provide random scattering. Rhodamine 6G dye in 2 - methyl - 2, 4 - pentanediol (MPD) solution was selected as the luminifor, and TiO_2 particles of 0.18 microns diameter were added to provide scattering. This is a similar combination to that previously used to study backscatter image enhancement in scattering media.[1]

Fluorescence, absorption, and excitation spectra measurements were carried out using transparent plastic cells of varying sizes containing mixtures of the dye solution and TiO_2 beads. Fluorescence was investigated for two different cell arrangements with front surface and side excitation as shown in (a) and (b), respectively, Fig. 3.8, using a Perkin Elmer Luminescence Spectrophotometer LS 50. The lamp in the spectrophotometer was used as a light source for excitation, the typical excitation wavelength was 514 nm.

3.4 Result and discussion

The intrinsic fluorescence of Rhodamine 6G, in $2x10^{-4}$ molar concentration in MPD was first obtained in a thin 0.016 cm x 1 cm cell by measuring front surface excitation. This is shown by the solid curve in Fig. 3.9(a). This measurement provides a standard for comparison. The same concentration of dye solution was then examined in 1 cm x 1 cm cells using both front surface and side excitation, with and without the addition of known concentration of scatterers. Fig. 3.9(a) show the results obtained, with the intrinsic fluorescence superimposed for comparison. The broken curve in Fig. 3.9(a) shows that the front surface fluorescence of the thick test cell of 1 cm thick is red shifted with respect to the intrinsic fluorescence (from 0.016 cm thick cell). This red shift is expected because in the thick cell, the fluorescence inside the solution contributes to the observed emission spectrum. Because of the longer path the fluorescence light has to propagate though the dye solution, the shorter wavelength region of the emission spectrum will be preferentially absorbed by the dye compared to that of the longer wavelength region. Thus, the resultant, fluorescence spectrum from a thick cell is red shifted, when compared to that from a thinner cell. This effect is further enhanced as shown by dot-dashed curve where an even bigger red shift results with the side excitation since the internally excited fluorescence now has on the average an even longer path to get to the viewing surface.

The effect of a random scattering medium on the fluorescence spectrum of the dye solution is presented in Fig. 3.9(b). The solid curve of Fig. 3.9(b) is the fluorescence spectrum of $2x10^{-7}$ M Rh6G in MPD in a 1 cm thick cell. This spectrum is itself blue shifted when compared with that for a considerably higher concentration (3 orders of magnitude) of dye solution,

shown by the broken curve of Fig.3.9(a). These observation illustrates the dependence of the fluorescence spectrum on dye concentration and the (expected) effects of self absorption. The addition of TiO_2 scatterers into the dye solution results in a red shift of the luminescence spectrum obtained with front surface excitation as shown in Figs 3.9(b) by the broken curve. This red shift arises from the longer "random walk" path that the internally excited fluorescence must now undergo in the scattering medium to reach the surface.

To examine whether wavelength dependence of particulate scattering plays a part in the observed effects, the fluorescence of the test cells without the scatterers was viewed through a cell containing scatterers. The fluorescence spectrum transmitted through the dye-free scattering medium was found to be unaltered. For this purpose the experimental studies were carried out with the arrangement shown in Fig. 3.10. In this arrangement fluorescence from the dye cell A of 1 cm thick containing $2x10^{-4}$ M Rhodamine 6G was transmitted through a cell B, without and with $Ti0_2$ particles suspended in MPD, but with no dye. The fluorescence spectrum from sample A as shown by the solid curve in Fig. 3.11, was found to be essentially unaltered by the presence of (TiO_2) scatterers in sample B through which the fluorescence light was allowed to pass. Note that this fluorescence spectrum is slightly different from that shown in Fig. 3.9(a). This is because the emitted fluorescence spectrum is highly dependent on the experimental geometry.

Using a spectro-photometer, a direct transmission (OD) through the 1 cm thick test cell containing TiO_2 scattering medium without a dye was also measured. The optical density (OD) did not show wavelength dependence from 550 to 650 nm. Both above results indicate that the wavelength dependence of light scattering in TiO_2 medium is negligible component in the

dye fluorescence spectrum observed at the surface, and hence is not a significant factor in the red shift observed in Fig. 3.9(b). The tests were repeated with Rhodamine 6G dye added to the cell, B, containing the scatterers, and as expected the red shift is now observed. This is shown by the broken curve of Fig. 3.11, confirming that the red shift in the observed fluorescence spectrum is indeed due to the increased "random walk" absorption occurring at the shorter wavelengths of the fluorescence reaching the surface.

To examine whether the introduction of the TiO_2 scattering beads may have affected energy levels and hence the intrinsic fluorescence emission spectrum of the Rhodamine 6G, a thin 0.016 cm x 1 cm test cell was used to study the fluorescence spectrum in the presence of TiO_2 scatterers. A thin test cell was used so that the long trajectory path for the fluorescence light which arises from the excitation of dye deep inside the cell, is no longer a factor. The intrinsic fluorescence spectrum of Rh6G ($3x10^{-7}$ M) obtained by front surface excitation fluorescence measurements is shown by the solid curve in Fig. 3.12. With the addition of TiO_2 scatterers to the solution there is a very small red shift shown by the broken curve Fig. 3.12. This implies that the larger red shifts observed in Fig.3.9(b) in thick cells (1 cm) are primarily due to increased absorption occurrence at the shorter wavelengths and, resulting from the increased "random walk" path length that the internally excited fluorescence emission in the 1 cm thick cell has to travel to reach the surface.

The effects of increased scatterer densities were also examined in the 0.016 cm x 1 cm cells that were used to obtain the results in Figs 3.9(b). Using the same dye concentrations, ($3x10^{-7}$M), the bead concentration was gradually increased and the front surface excitation fluorescence monitored

for different concentrations. As the bead concentration was increased, it was observed that the red shift in the observed fluorescence peak increased. A maximum shift of the peak of up to 7 nm was being observed at bead concentrations of $6.35 \times 10^{12}/cm^3$, Fig. 3.9(b). As the bead concentration was further increased, the red shift was observed to decrease. At a bead concentration of $1.2 \times 10^{13}/cm^3$, the peak of the fluorescence spectrum shown by the dashed line (with scatterers) is 4 nm blue-shifted vs. the solid line, as shown in Fig. 3.13. Both these effects may be understood qualitatively in the following manner. As the scattering bead concentration is initially increased, the internally emitted fluorescence undergoes an increase in the length of the "random walk" it takes to get to the surface, and hence undergoes more absorption resulting in an increase in red shift. This effect predominates, until the increase in scatterers concentration has reached the point where it starts to greatly inhibit penetration of the excitation radiation, and hence excitation and fluorescence emission are both restricted to take place nearer the surface, with the length of random walks to the surface being consequently shortened and self absorption and red shift lessened. There are thus two competing effects at work.

The excitation spectra of a dye solution will also be significantly affected by the presence of scatterers. The curves presented in Fig. 3.14 show the excitation spectra of DCM in MPD observed at 630 nm using side excitation (Fig. 1). The observed excitation spectra in the absence of TiO_2 scatterers is shown by the solid curve showing two absorption bands at 300 to 420 nm and 530 to 590 nm which contribute to emission at 630 nm. The contribution of 300 to 420 nm absorption bands is significantly reduced in the presence of TiO_2 scatterers. This could be due to the either increased scattering and/or absorption of ultraviolet light by the TiO_2 scatterer which reduces the amount

of excitation light reaching the dye. In the presence of scatterers, the relative contribution of the excitation at 400 to 520 nm band increases as the density of scatterer increases. This observation attributed to the random walk process of the excitation light in the scattering medium. For the less absorbing excitation light, such as 400 to 520 nm band, the scatter effectively increases the length of photon travel in the medium and therefore the interaction of the excitation light with the dye. This in turn increases absorption and excitation in this relatively weakly absorbing 400 to 520 nm spectrum, and therefore increases the observed fluorescence. Fig. 3.14 also shows that the excitation 520 to 590 nm band is reduced, where the dye absorption is stronger. This observation shows that the relative amount of absorption for stronger absorbing band is reduced with respect to the weaker absorbing band in a highly scattering medium. This is because the weaker absorbing light needs the longer random path to enhance the absorption.

3.5 Conclusion

In conclusion, it is shown that the presence of random scattering in luminescent bodies will affect the spectrum of the fluorescent radiation observed at the surface of these bodies. The primary effects observed are red shifts in the emission spectra with respect to the intrinsic fluorescence emission. These shifts may be understood in terms of increased random walk, and hence increased in absorption that emission internally excited within the luminescent body undergoes when random scattering processes are introduced.

REFERENCES

1. K.M. Yoo, Z.W. Zang, S.A. Ahmed, and R.R. Alfano, "Imagine objects hidden in scattering media using a fluorescence-absorption technique", Opt.Lett.16,1252-54 (1991).
2. D.B. Tata, M. Foresti, J. Cordero, P. Tomashefsky, M.A. Alfano, and R.R. Alfano,"Fluorescence polarization spectroscopy and time-resolved fluorescence kinetics native cancerous and normal rat kidney tissues," Biophys.J.Biophys.Soc.50, 463-469 (1986).
3. Y.L.Yang, Y.M. Ye, R.M. Li, Y.F. Li, and P.Z. Ma, "Characteristic autofluorescence for cancer diagnosis and its origin," Laser Surg. Med. 7, 528 (1987).
4. S. Montan and L.G. Stroemblad, "Spectral characterization of brain tumors utilizing laser-induced fluorescence," Lasers Life Sci. 1, 275-285 (1987).
5. B.L. Horecker, "The absorption spectra of hemoglobin and its derivatives in the visible and near infra regions," J. Biol. Chem. 148, 173-183 (1943).
6. J. Martorell and N.M. Lawandy "Spontaneous emission in a disordered dielectric medium". Phys. Rev. Lett. 66, 887-890 (1991).
7. S.A. Ahmed, Z.W. Zang, K.M. Yoo, M.A. Ali, and R.R. Alfano, Appl. Opt., Vol. 33, No. 13, 2746-50 (1994).
8. N.G. Bakhshiev, Opt. Spectrosc. Vol 32, PP. 1151 (1972).
9. N.G. Bakhshiev and B.S. Neporent, Opt. Spectrosc. Vol. 16, PP. 191 (1970)
10. P. P. Sorokin and J. R. Lankard, IBM J Research and develop. Vol. 10, pp. 162-163, March (1966).
11. F. P. Shafer, W. Schmidt, and J. Volez Vol. 9, pp. 306-309, October

(1966).

12. M. L. Spaeth and D. P. Bortfield, Appl. Phys. Letters, Vol. 10, pp. 179-181, September (1966).
13. P. P. Sorokin and J. R. Lankard, IBM J. Research and Develop. Vol 11, pp. 148, March (1967).

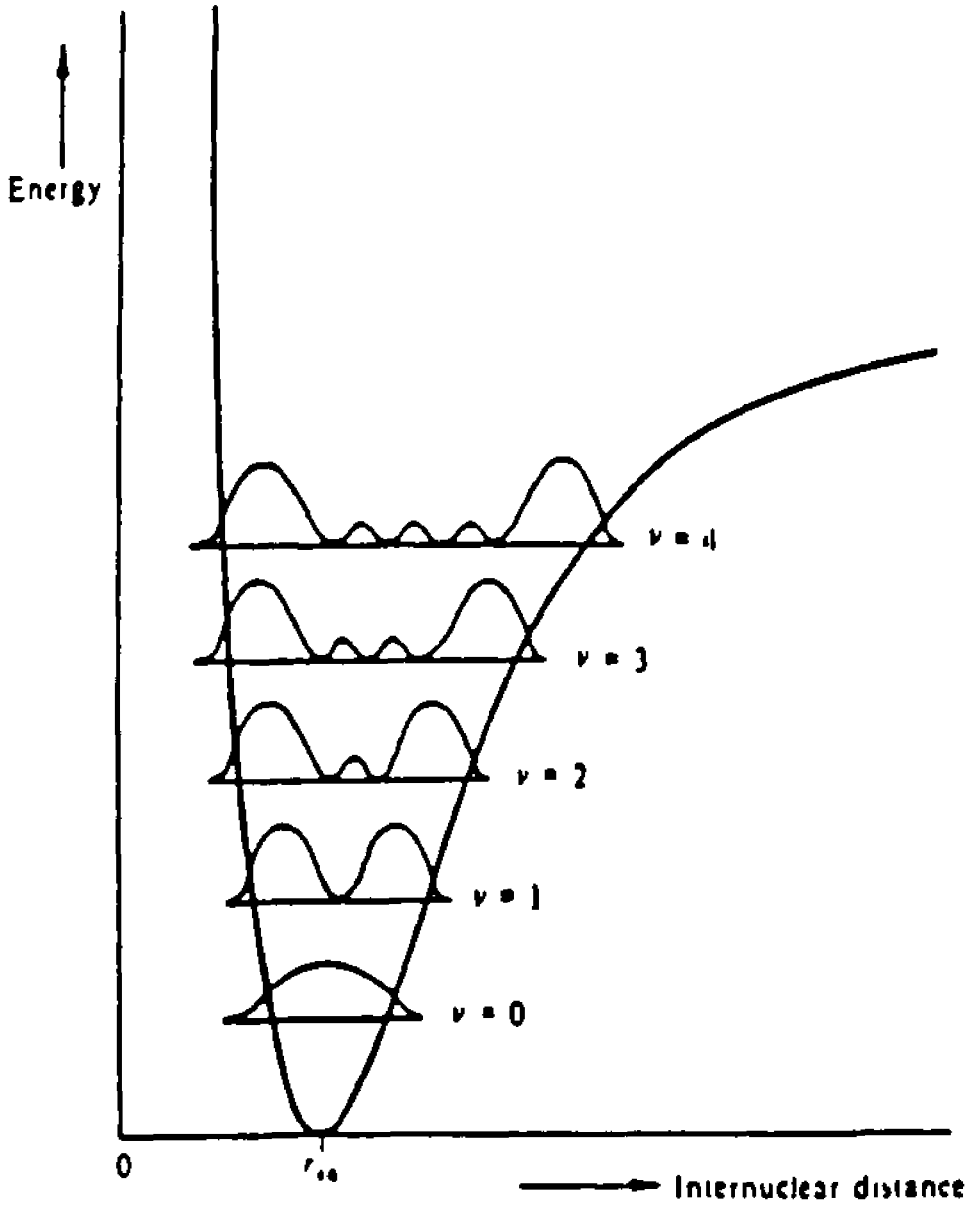

Fig. 3.1 The probability distribution for a diatomic molecule according to the quantum theory. The nuclei are most likely to be found at distances apart given by the maxima of the curve for each vibrational state.

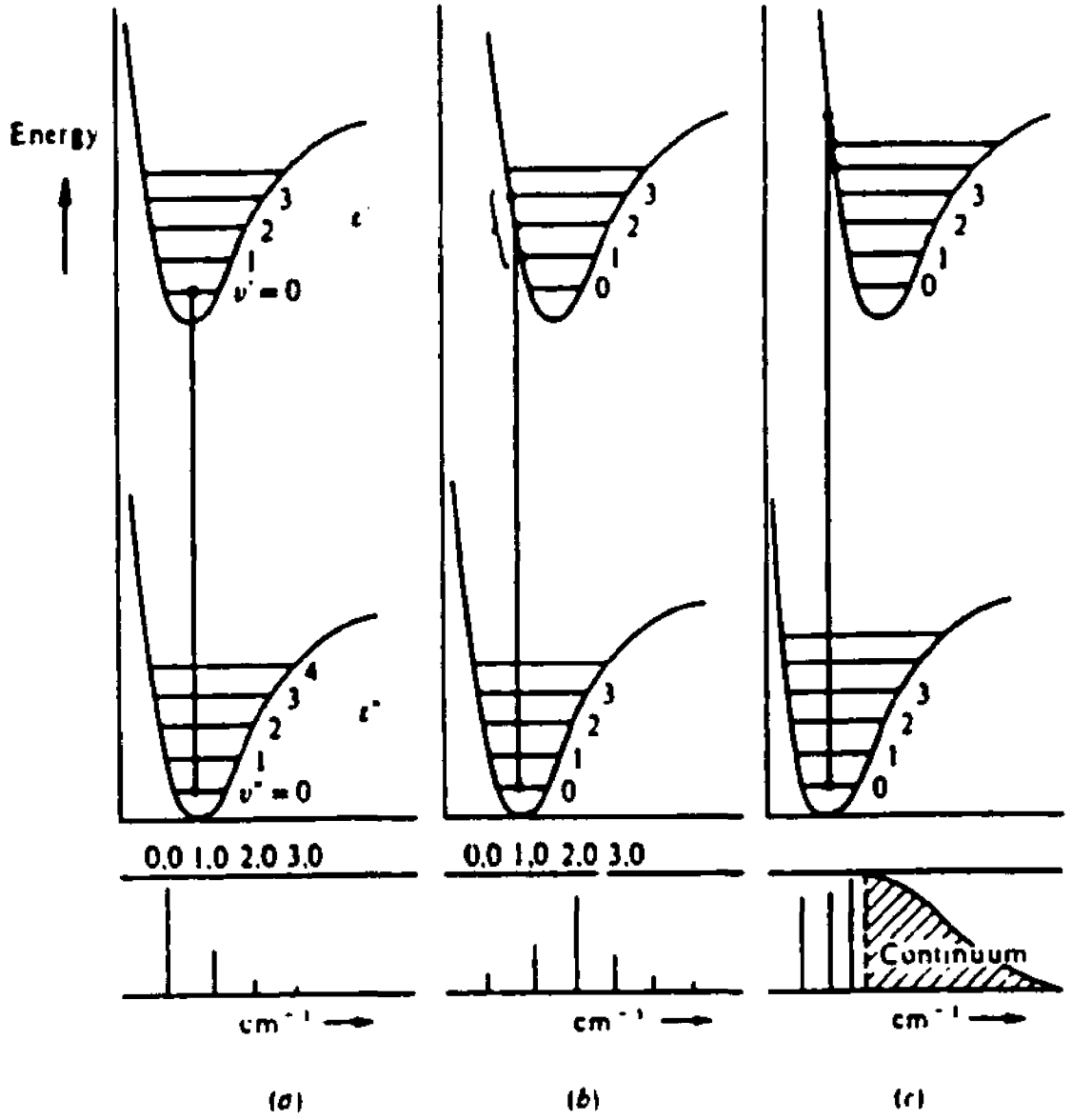

Fig. 3.2 The operation of the Franck-Condon principle for (a) internuclear distances equal in upper and lower states, (b) Upper state internuclear distance a little greater than that in the lower state, and (c) Upper state distance considerably greater.

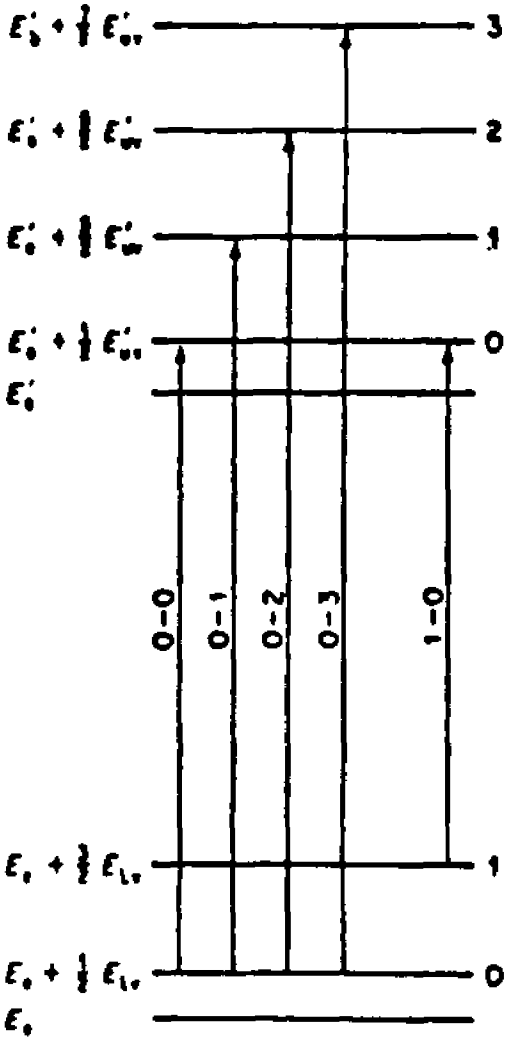

Fig. 3.3 Vibronic absorption transitions.

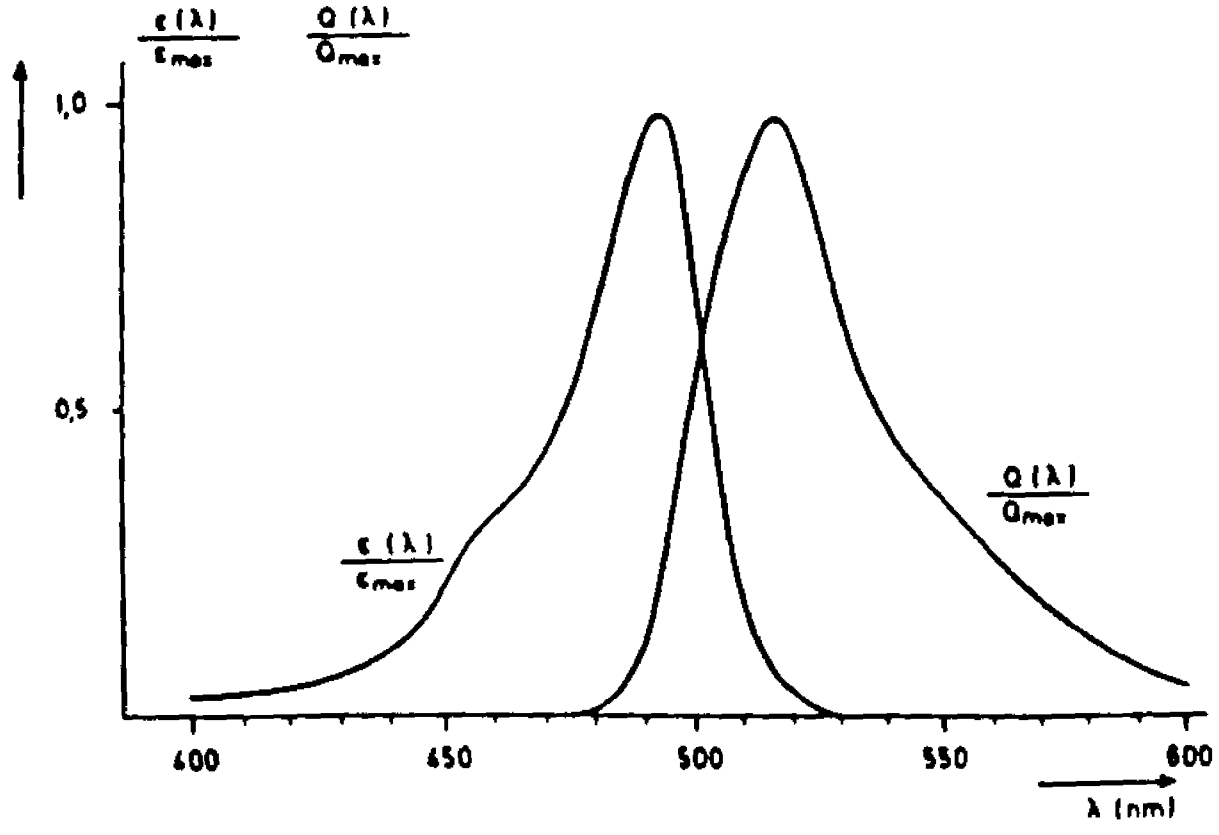

Fig. 3.4 Absorption spectrum, $\varepsilon(\lambda)/\varepsilon_{max}$, and fluorescence spectrum, $Q(\lambda)/Q_{max}$, of a typical dye molecule.

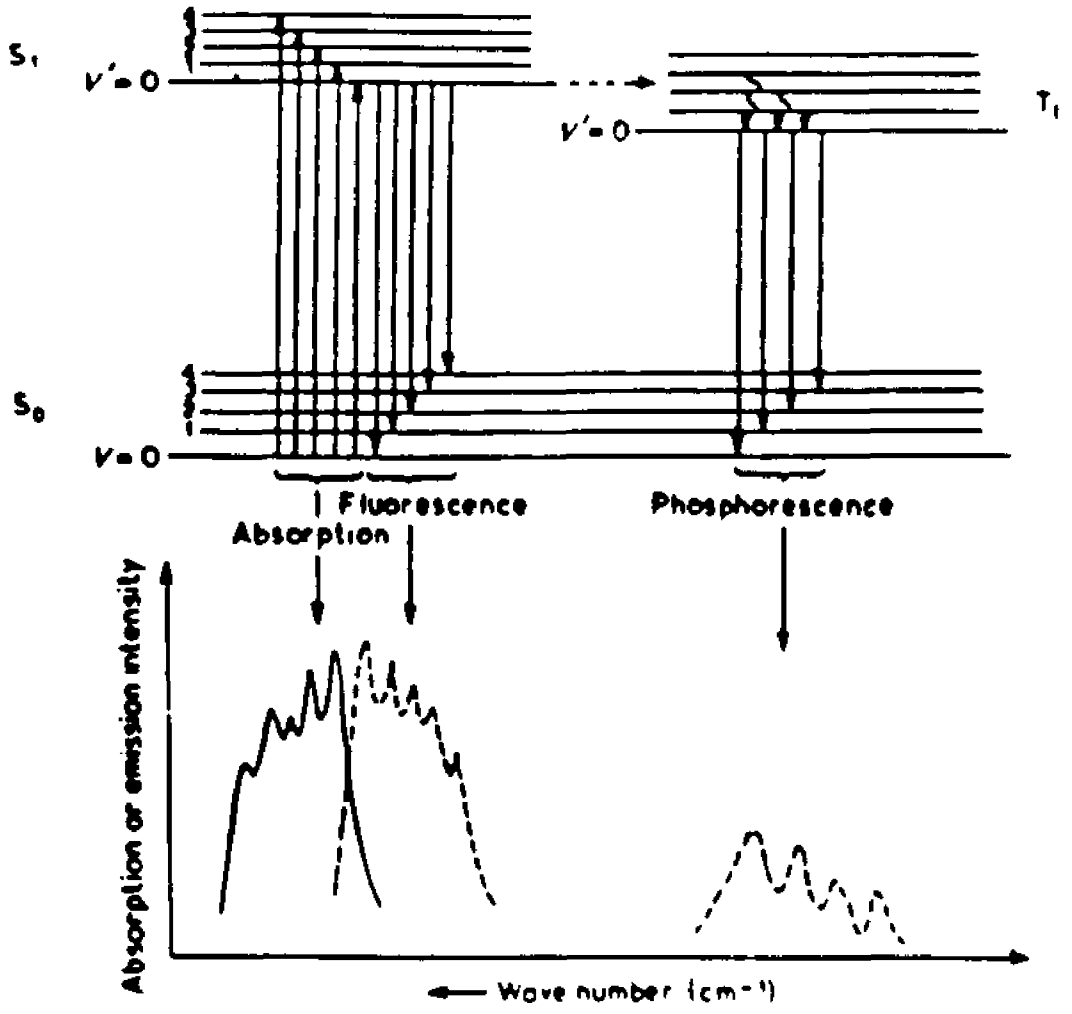

Fig. 3.5 Origin of absorption, fluorescence and phosphorescence spectra.

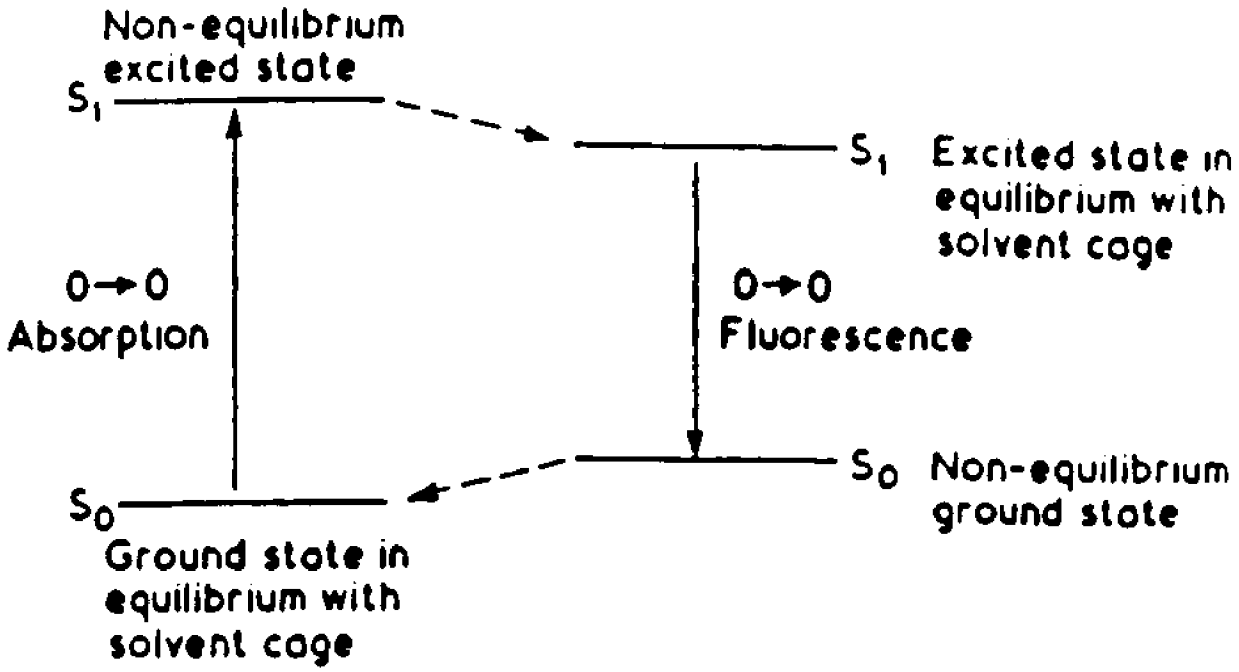

Fig. 3.6 Solvent equilibrium on energy of electronic states.

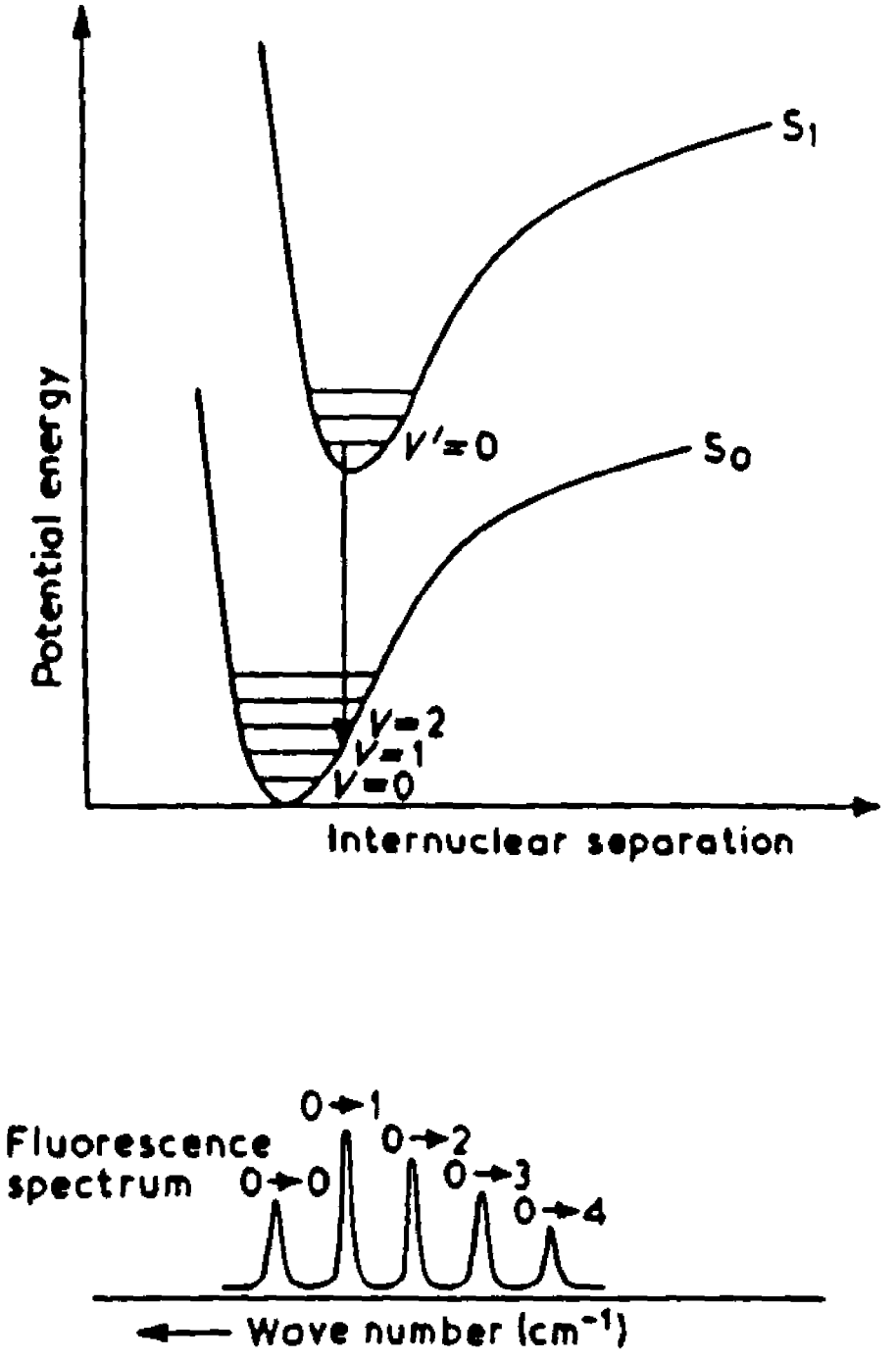

Fig. 3.7 Representation of the fluorescence spectrum of a diatomic molecule showing possible relative intensities of the vibrational bands.

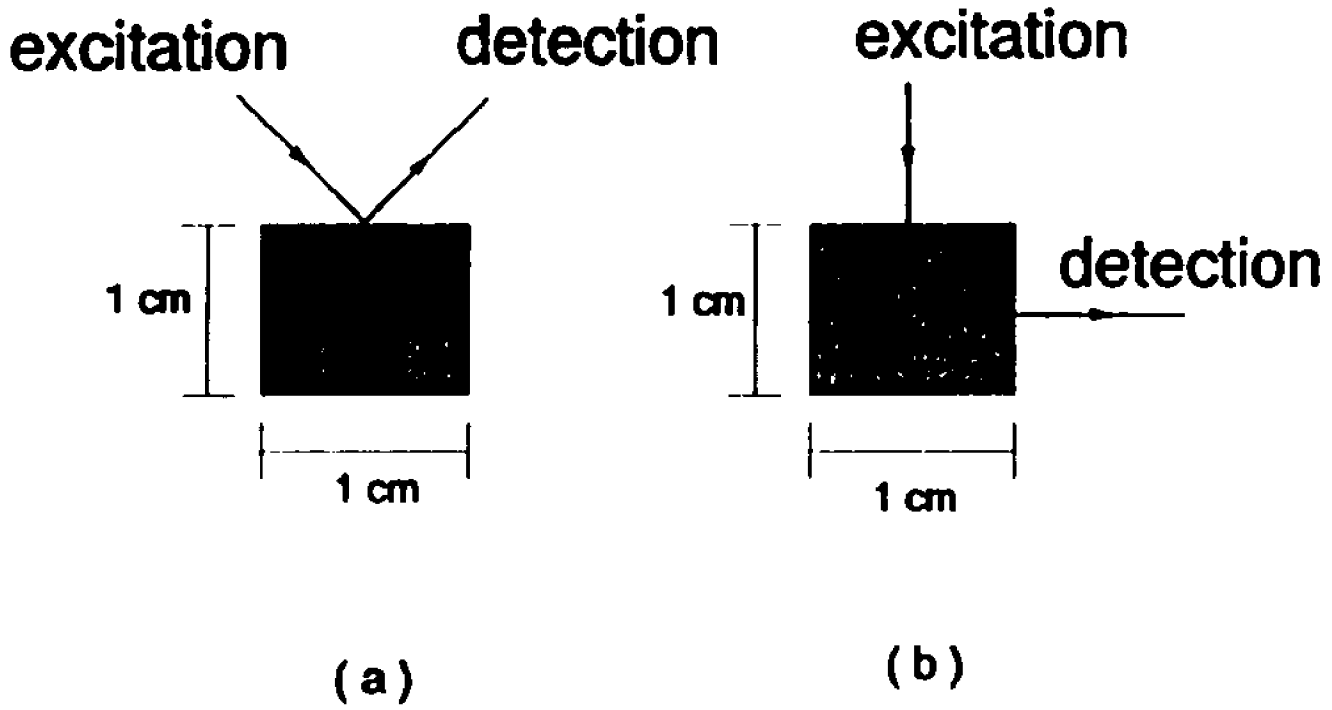

Fig. 3.8 The excitation and detection arrangement of fluorescence of dye in a transparent plastic cell.

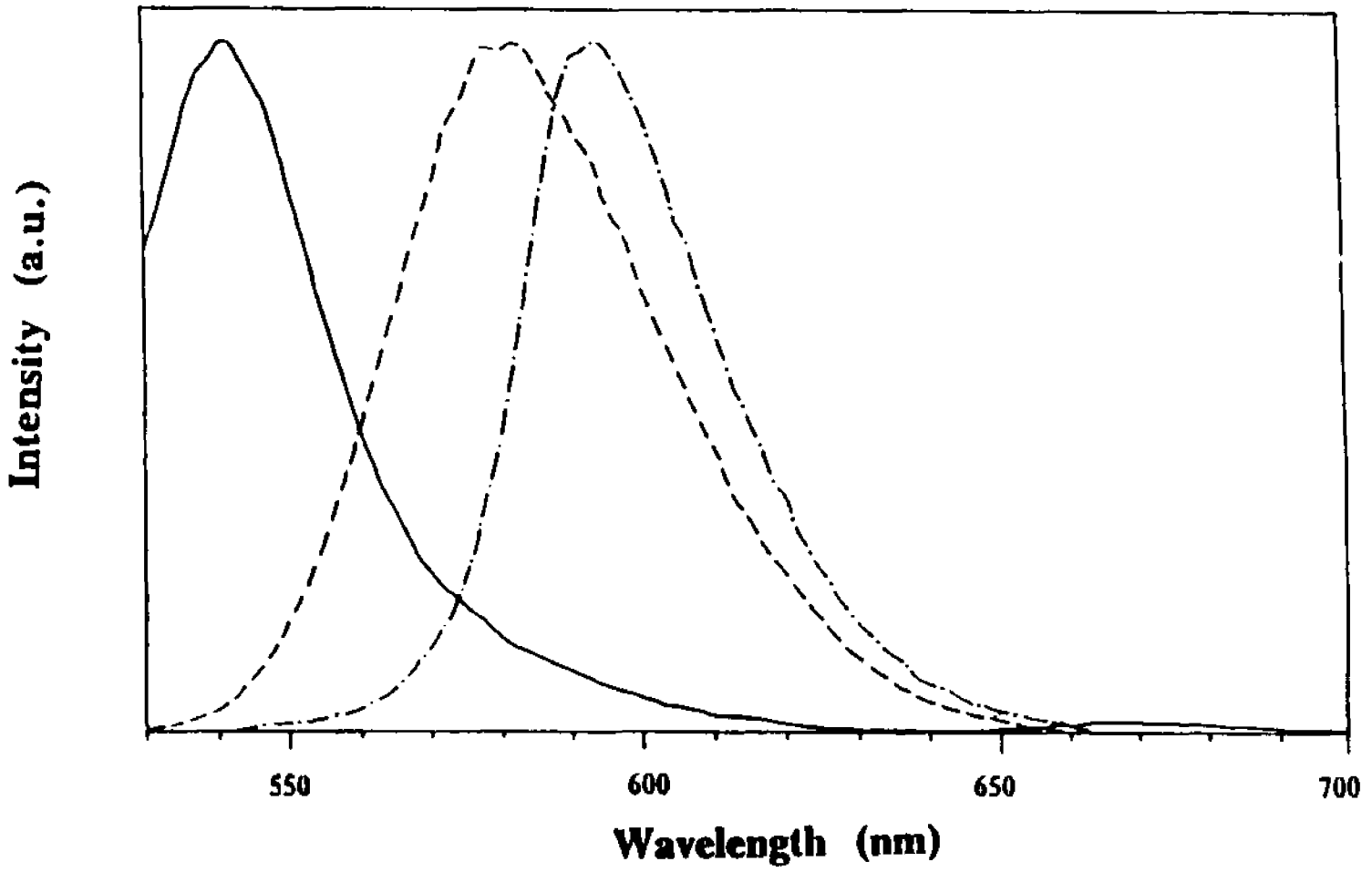

Fig. 3.9(a) The fluorescence spectra of 2×10^{-4}M Rh 6G in 2 methyl-2.4-pentanediol (MPD) solution. Solid curve: front surface detection from 0.16 cm thick cell; broken curve: front surface detection from 1 cm thick cell; dashed dot curve: side surface detection from 1 cm thick cell.

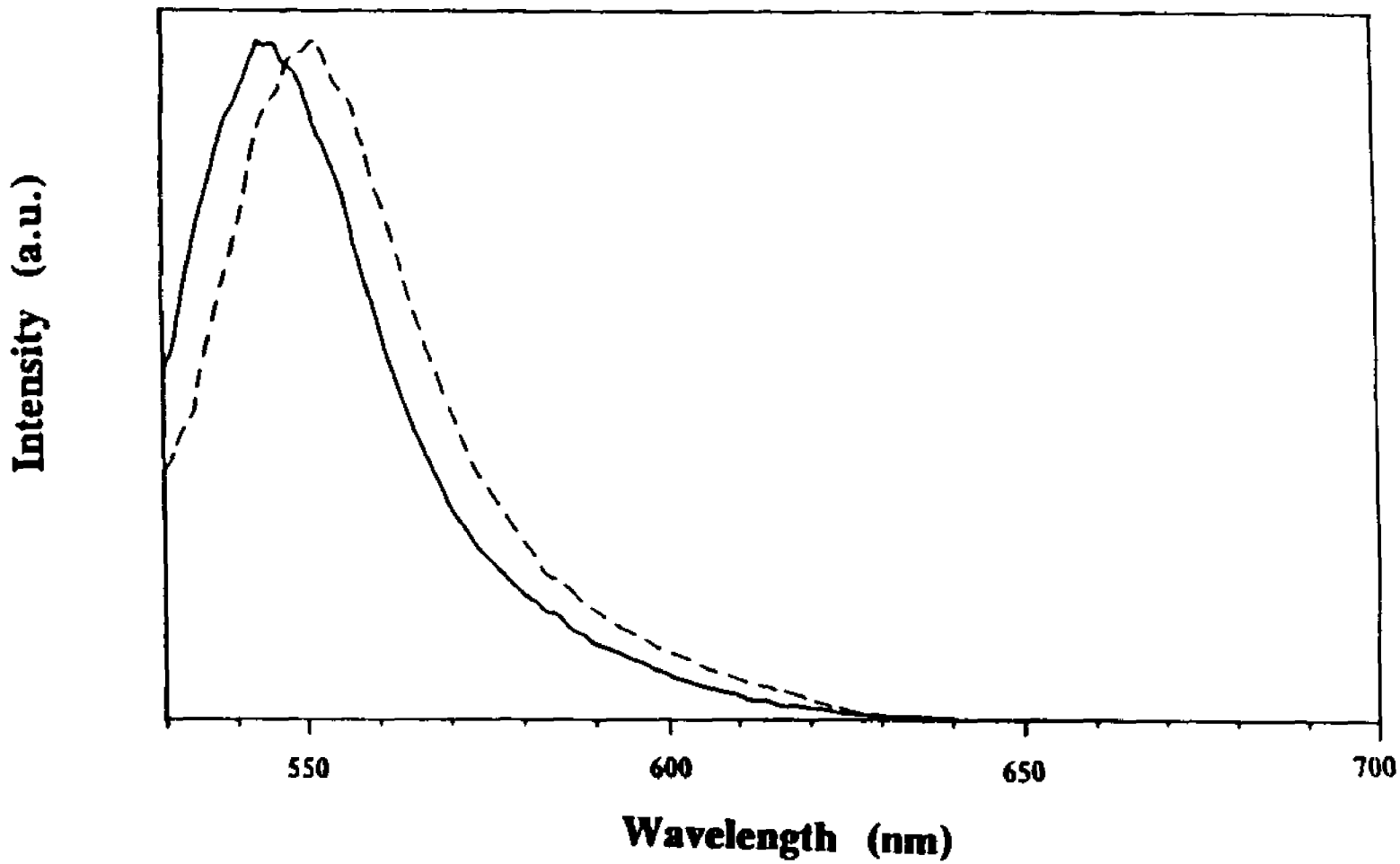

Fig. 3.9(b) Fluorescence spectra of front surface detection from a 1cm thick cell of 2×10^{-7} M Rh 6G in MPD. Solid curve: dye solution; broken curve: dye solution plus TiO_2 scatterers.

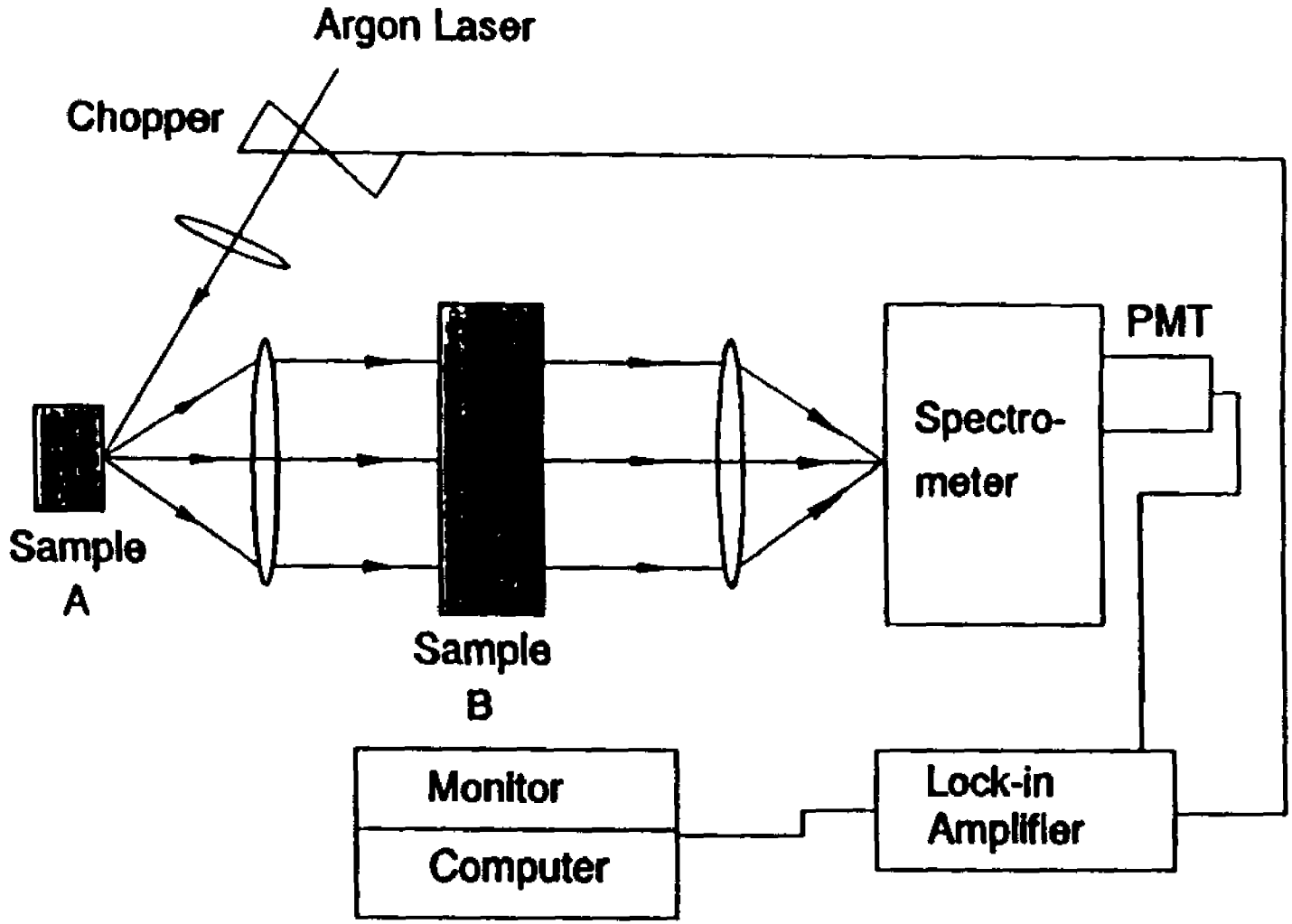

Fig. 3.10 Schematic of experimental setup to study the effect of the fluorescence spectrum when passing through a dye and a scattering medium.

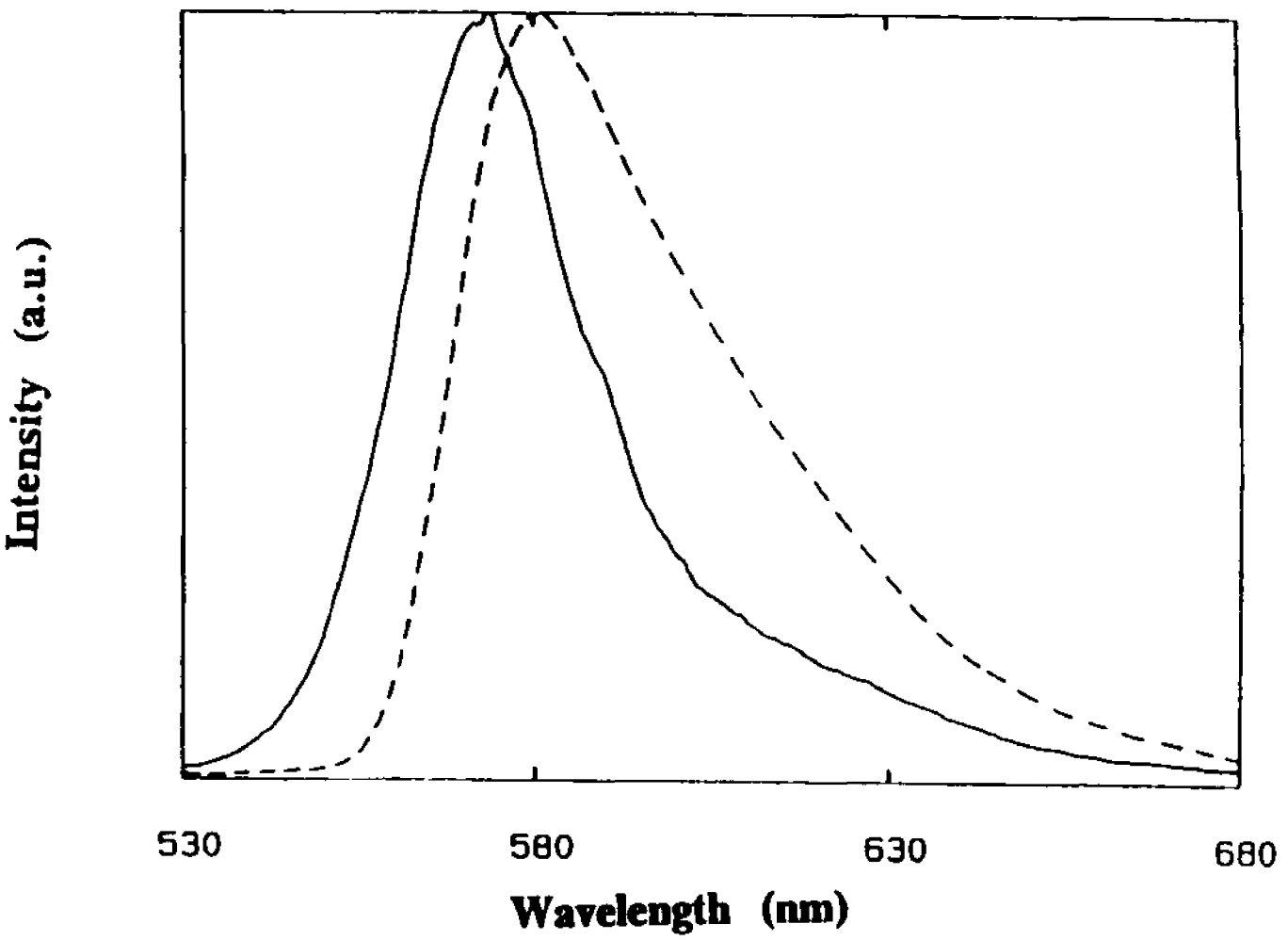

Fig. 3.11 The spectra of a fluorescence spectra (from 2×10^{-4} M Rh 6G in 1cm thick cell) when it passes through a sample consisting of: solid line: both no scatter and with TiO_2 scatterer in the MPD; broken line: TiO_2 in MPD with Rh 6G dye (2×10^{-4} M).

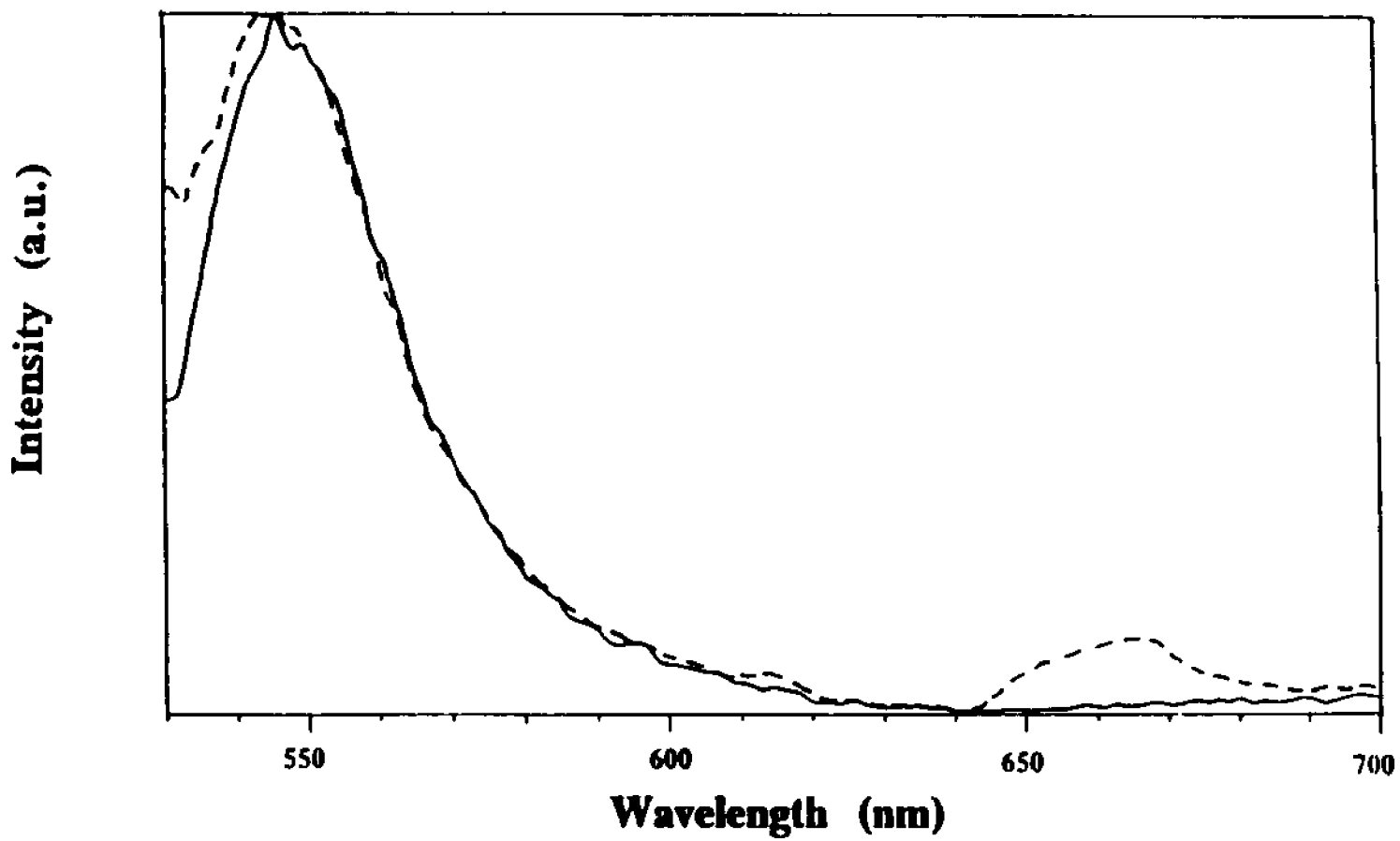

Fig. 3.12 Comparison of (thin 0.016 cm) cell dye (3×10^{-7} M) fluorescence with and without scatterers. Solid line: dye fluorescence; broken line: dye with scatterers fluorescence.

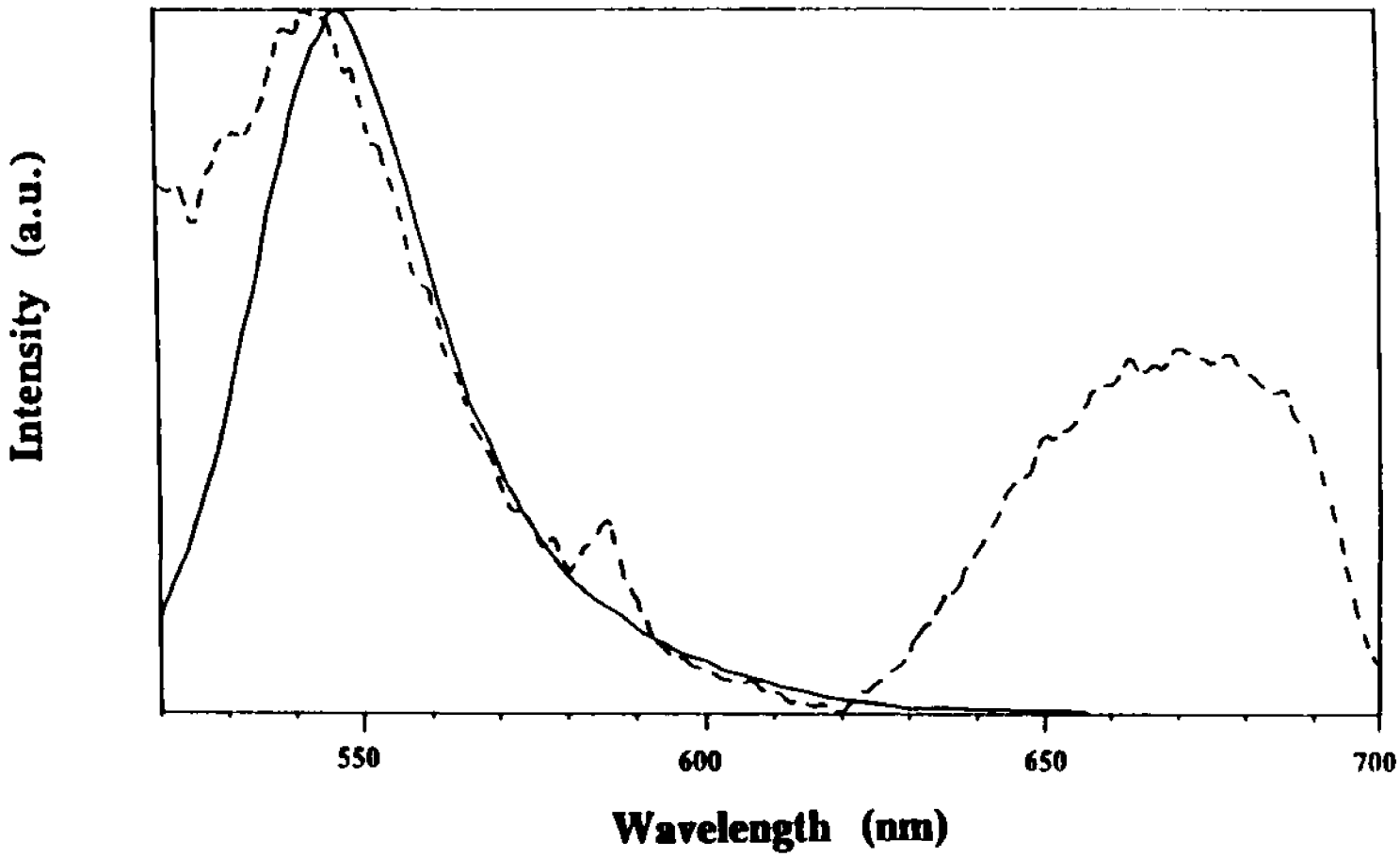

Fig. 3.13 Comparison of dye (3×10^{-7} M) and dye with scatters' fluorescence of maximum blue shift in (thick 1cm) cell. Solid line: dye fluorescence; broken line: dye with scatters' fluorescence.

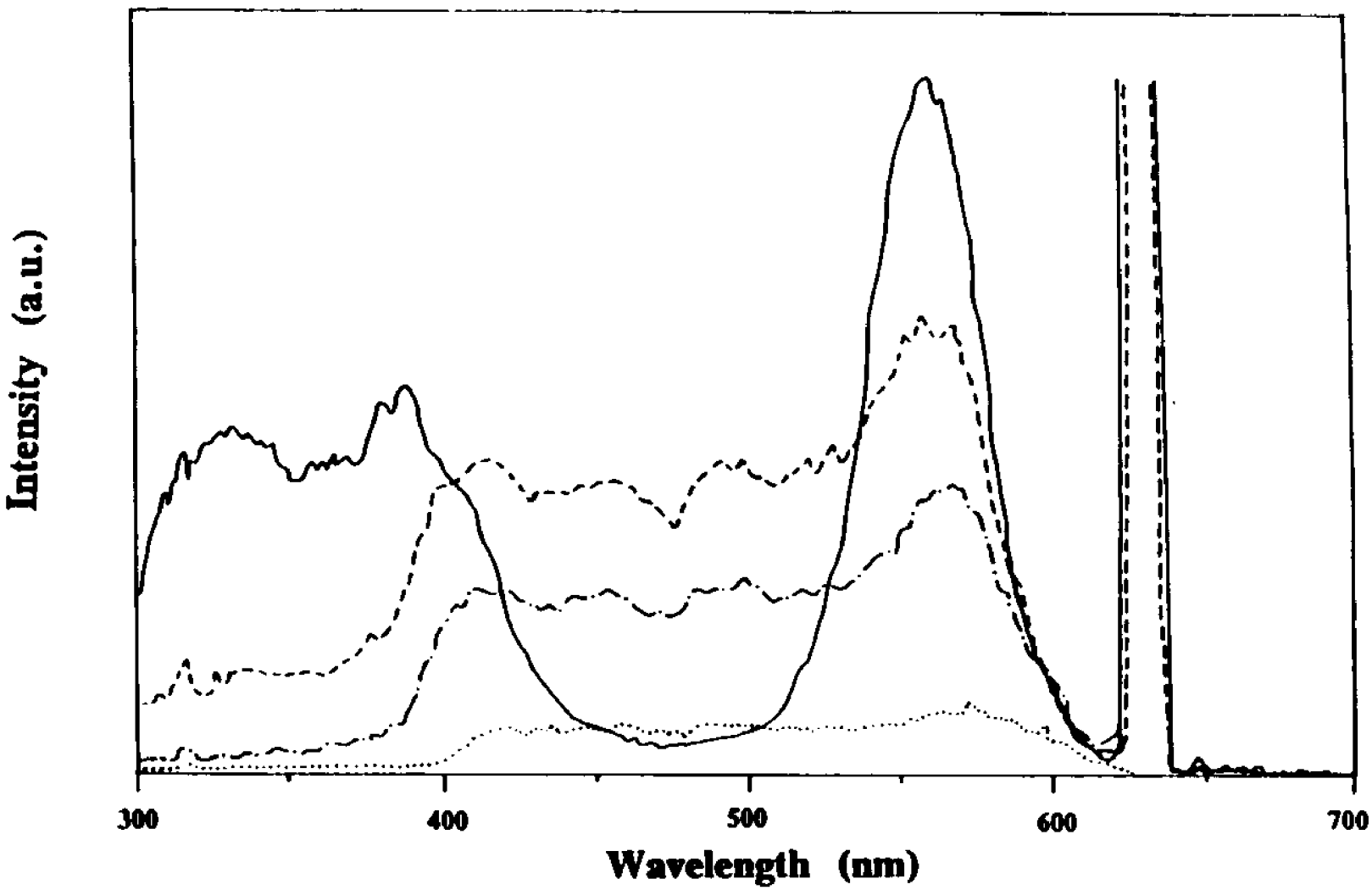

Fig. 3.14 Comparison of excitation spectra of dye DCM (2.6×10^{-4} *M*) and dye with increasing scatters. Solid line: dye fluorescence; broken line: dye with 0.005 g scatters fluorescence; dashed dot line: dye with 0.009 g scatters fluorescence; dotted line: dye with 0.039 g scatters fluorescence.

IV. DNA Ploidy Measurements in Breast and Colon Cancer using Fluorescence Image Cytometry

4.1. Introduction

DNA measurements are of great importance in the analysis of cancer cells. Several techniques have been developed to perform these measurements during the last two decades, most notable is the flow cytometry technique (FCM)[1-3] which is currently in use for clinical diagnosis. Another technique which has gained importance in recent years is the fluorescence image cytometry technique (FIC)[3-6]. FIC is a slide based microscopy technique for making quantitative measurements on florochrome stained cellular specimen. The specimen is irradiated by an excitation source, usually a Hg lamp, the emitted fluorescence is imaged by the microscope onto a CCD camera, then digitized, stored, and analyzed by a computer. FIC has been shown to be important in studies where a specimen contains too few cells for FCM.[5] Additionally, a broad variety of measurements of the cells and their components can be obtained (e.g. area, perimeter, and texture)[6], allowing a highly detailed study of individual cell or families of cells in order to provide a diagnostic opinion. A disadvantage of FIC is that it is extremely time intensive, however, automated image acquisition systems can alleviate this problem to some extent.[7] Another advantage of FIC over techniques such as FCM or densitometry is that several simultaneous images of specimen tagged with spectrally distinct labels can be obtained allowing quantification of several markers in the same cell.[8]

In this report, we employ the use of the FIC technique to measure DNA ploidy of breast and colon cancer specimens, stained with propidium iodide, axially illuminated by an Argon laser at 488 nm, and imaged by a Leitz microscope onto a computer controlled CCD camera and image processing system capable of feature extraction and DNA fluorescence image histogram analysis. The laser illumination has the advantage of uniformity

over the field of view of the microscope as well as reproducible power stability. Additionally, the excitation wavelength can be matched to the DNA tag to improve fluorescence efficiency and avoid possible interfering background emission. Results from FCM on the same specimens are presented for comparison.

4.2. Experimental Method

We studied samples of cancerous and normal tissue from patients operated on at the Mount Sinai Medical Center of New York. The tissue was fresh, without fixation, stored in a freezer at -70 ℃ , defrosted at room temperature, minced, filtered (53 and 37 microns), added to bovine serum 5% and washed by centrifugation (12000/10 minutes/4 ℃). After pouring the supernatant, RNA-ase and Propidium Iodide dye were added and incubated for 30 minutes, then filtered and analyzed.

Our FIC system consists of the following: an argon laser, a microscope, a CCD camera, a personal computer with a frame grabber board, and monitor. In our experiment, stained nuclei were smeared on a glass slide, illuminated axially from below by the laser beam at λ = 488 nm. The laser was operated in the light control mode which kept the output power constant. The incident beam and fluorescence light emitted by cell samples were collected by the microscope with a Shott OG550 sharp cut-off barrier filter which transmitted the fluorescence and cut off the laser light. The fluorescence image of the sample was captured by a color CCD camera and sent to an image processing system to calculate the integrated relative fluorescent intensity and the size of the cells.

4.3. Result and Discussion

Both normal and cancer tissue samples were measured using the FIC system. The amount of DNA/dye was quantified by integrating the fluorescence from each pixel inside a nucleus image. Histograms for both cancerous and normal samples were obtained. As the amount of dye attached onto a cell nucleus, and hence the amount of fluorescence, is proportional to the amount of DNA, the total DNA content of a cell nucleus can be determined from its total integrated fluorescence intensity. Figure 4.1 shows the histogram of 122 normal cells (lymphocytes) which have a diploid or normal amount of DNA. This histogram provides a standard for comparison. Also shown is the histogram of 100 breast cancer cells which have a hyperdiploid amount of DNA, and a histogram of 128 colon cancer cells which have a hypodiploid amount of DNA. In this same way, we measured eleven other cancerous (breast and colon) and two other normal (lymphocytes) samples with similar results to those shown in Figure 4.1.

Besides intensity measurement, the area and perimeter measurement of fluorescent nuclei were also conducted on the same cell samples as above. Figure 4.2 shows the area histograms comparison of the normal and cancer cells. Figure 4.3 shows the trace histograms comparison. Both area and trace histogram figures show similar distributions for the cancer and normal cells as those obtained in the intensity histograms. Again, cancerous specimens display a distribution distinct from that of the normal specimens, with the peak of the histogram shifted to the lower or higher magnitude side. This similarity of the results demonstrated the correlation of cell area and perimeter to the amount of DNA in the cell.

Fluorescence intensity distributions within the nuclei in the specimens considered showed a more scattered distribution pattern for cancer cells than normal cells, however, no distinct features were clear.

A comparison was made with flow cytometry results obtained from Mount Sinai Medical Center and our FIC results. The same cancer tissues were measured by both techniques. Figure 4.4 shows the histograms of the breast and colon cancer cells obtained by the flow cytometry technique, which can be compared with FIC result as shown in Figure 4.1. Note that in Figure 4.4(a), the first peak is that of normal cells such as lymphocytes cells that are intermingled with tumor cells. The second peak is that of cancer cells. In the flow cytometry measurement, a total of approximate 20,000 nuclei were included in the histogram, and the DNA index was measured to be 1.94. In FIC, only 100 nuclei were analyzed, the calculated DNA index was 1.70. Figure 4.4(b) shows the histograms of colon cancer cells obtained by the flow cytometry technique, which can be compared with FIC result as shown in Figure 4.1. In this figure, the normal peak is the one to the left. The DNA index was 0.59 in flow cytometry, and 0.53 in FIC. It is apparent that FIC yields comparable DI values to flow cytometry.

4.4. Conclusion

DNA ploidy measurements of nuclei obtained by FIC for DNA index analysis show that cancerous specimens display a distinct distribution relative to the normal specimens, with the peak of the distribution shifted to lower or higher intensity, demonstrating deviations in the DNA content with respect to the normal. Additionally, in the case of the breast cancer specimen, the width of the distribution is more than twice that for the normal cells. A correlation between the cell morphology (area and perimeter) and DNA content (integrated fluorescence) was demonstrated for the samples studied.

The use of a laser source for FIC studies has several advantages including uniformity of illumination due to the superior spatial quality of a

laser , as well as steady output power and efficient excitation of only the DNA stain of interest.

REFERENCES

1. L. G. Dressler, M. Bartow, and S. A. Bartow, "MD Seminars in Diagnostic Pathology", Vol6,No.1 pp55-82 (1989).
2. H. M. Shapiro, "Practical Flow Cytometry" , Alan R. Liss, Inc., New York, 1988.
3. P.S. Oud, A.G.J.M. Hanselaar, M.M.M. Pahlplatz, J.W.R. Meijer, and G. Peter Vooijs," Image DNA-Index (ploidy) Analysis in Cancer Diagnosis", Appl.Opt. 26, p.3349 (1987).
4. W. L. Parry and G. P. Hemstreet., "Cancer Detection by Quantitative Fluorescence Image Analysis", J. Urol. 139, pp 270-274 (1988).
5. B. R. Lee, B. D. Haseman, C. P. Reynolds, " A Digital Image Microscopy System for Rare-event Detection Using Fluorescent Probes", Cytometry 10, pp. 256-262 (1989).
6. S. I. Sato, H. Ito, H. Inaba, Y. Taguchi, and M. Kasai, "Highly Sensitive Fluorescence Microscope System for Single Biological Cell Using Laser Excitation and Digital Image Processing and Display", Opt. Quantum Electronics 18(1), pp. 81-84 (1986).
7. S. J. Lockett, K. Jacobson, M. O'Rand, D. G. Kaufman, M. Corcoran, M. G. Simon, H. Taylor, and B. Herman, "Automated Image-based Cytometry with Fluorescence-stained Specimens." Biotechniques 10, pp 514-519 (1991).
8. R. Debiasio, G. R. Bright, L. A. Ernst, A. S. Waggoner, and D. L. Taylor, "Five-parameter Fluorescence Imaging: Wound Healing of Living Swiss 3T3 Cells.", J. Cell Bio. 105, pp 1613-1622 (1987).

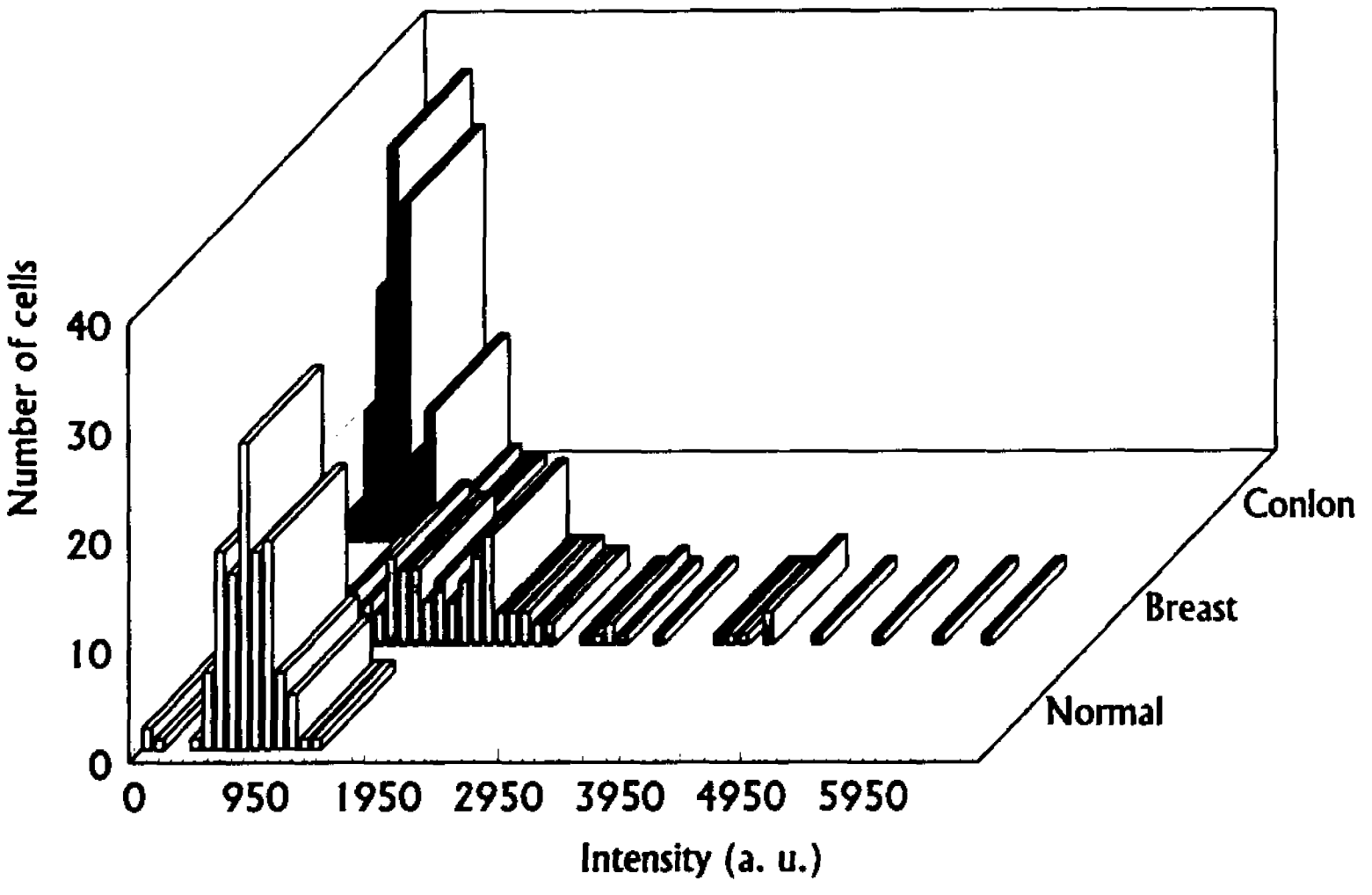

Fig. 4.1 Histograms of fluorescence intensity for normal(lymphocytes), breast cancer, and colon cancer specimen

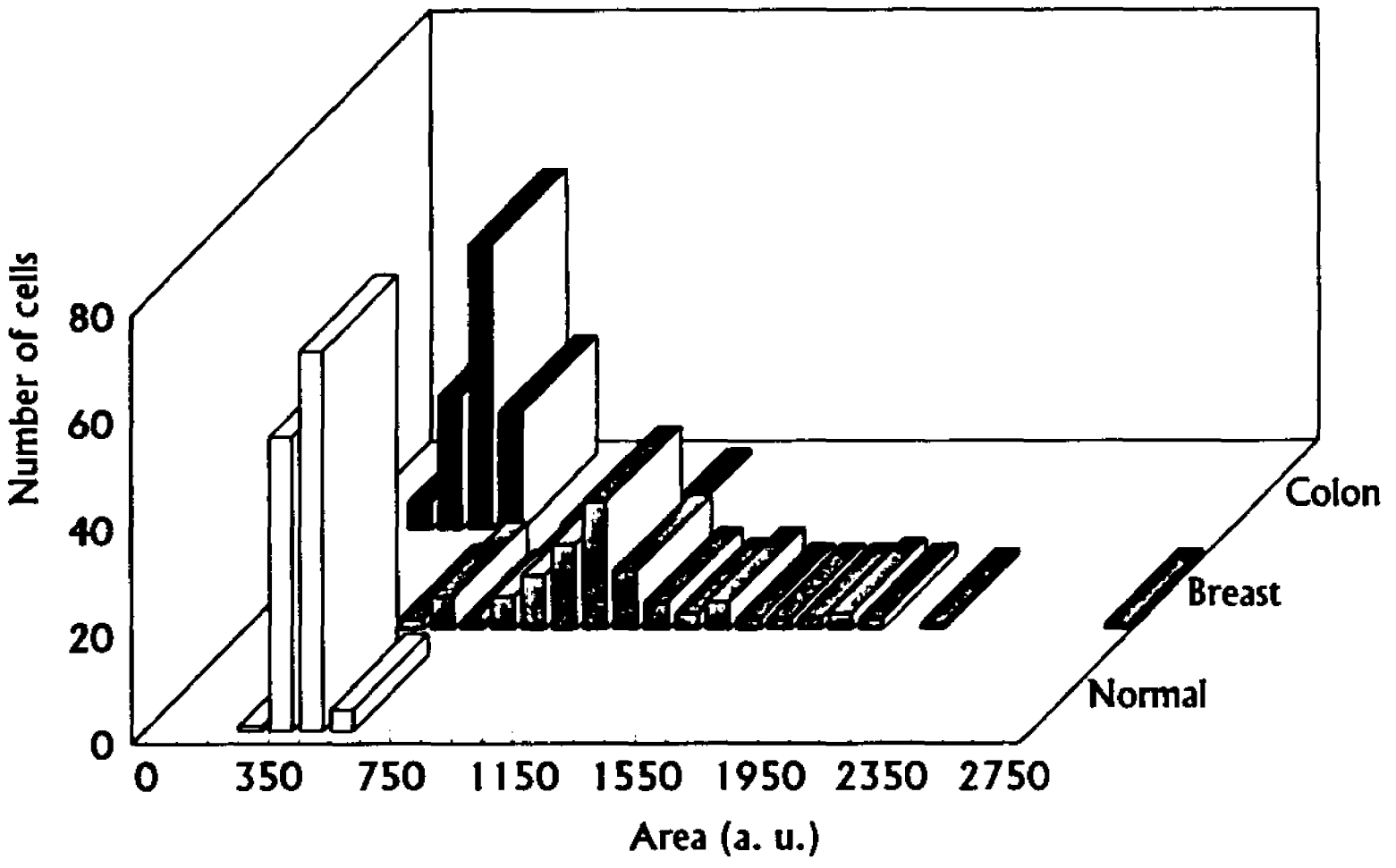

Fig. 4.2 Histograms of nuclei area for normal(lymphocytes), breast cancer, and colon cancer specimen

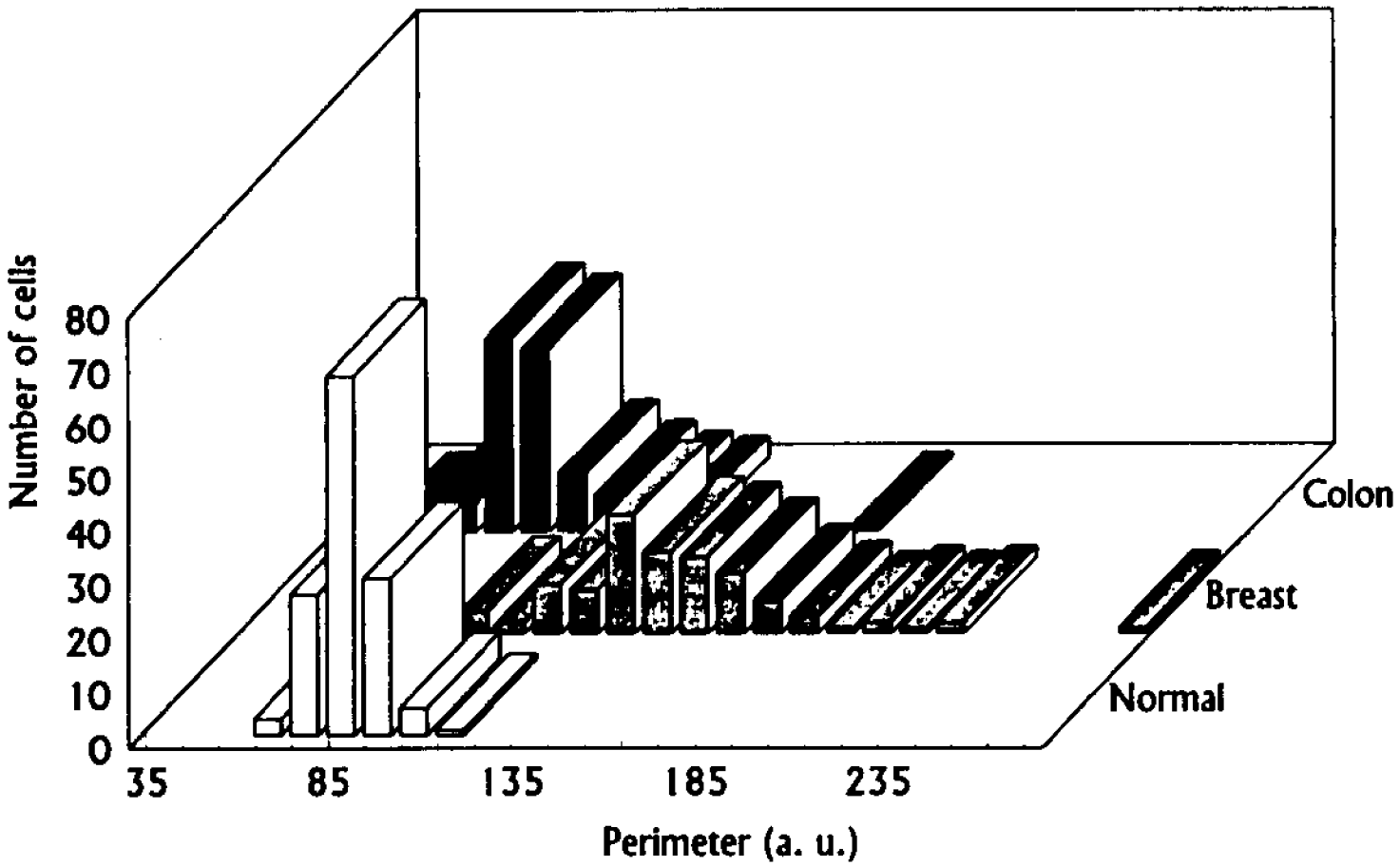

Fig. 4.3 Histograms of nuclei perimeter for normal(lymphocytes), breast cancer, and colon cancer specimen

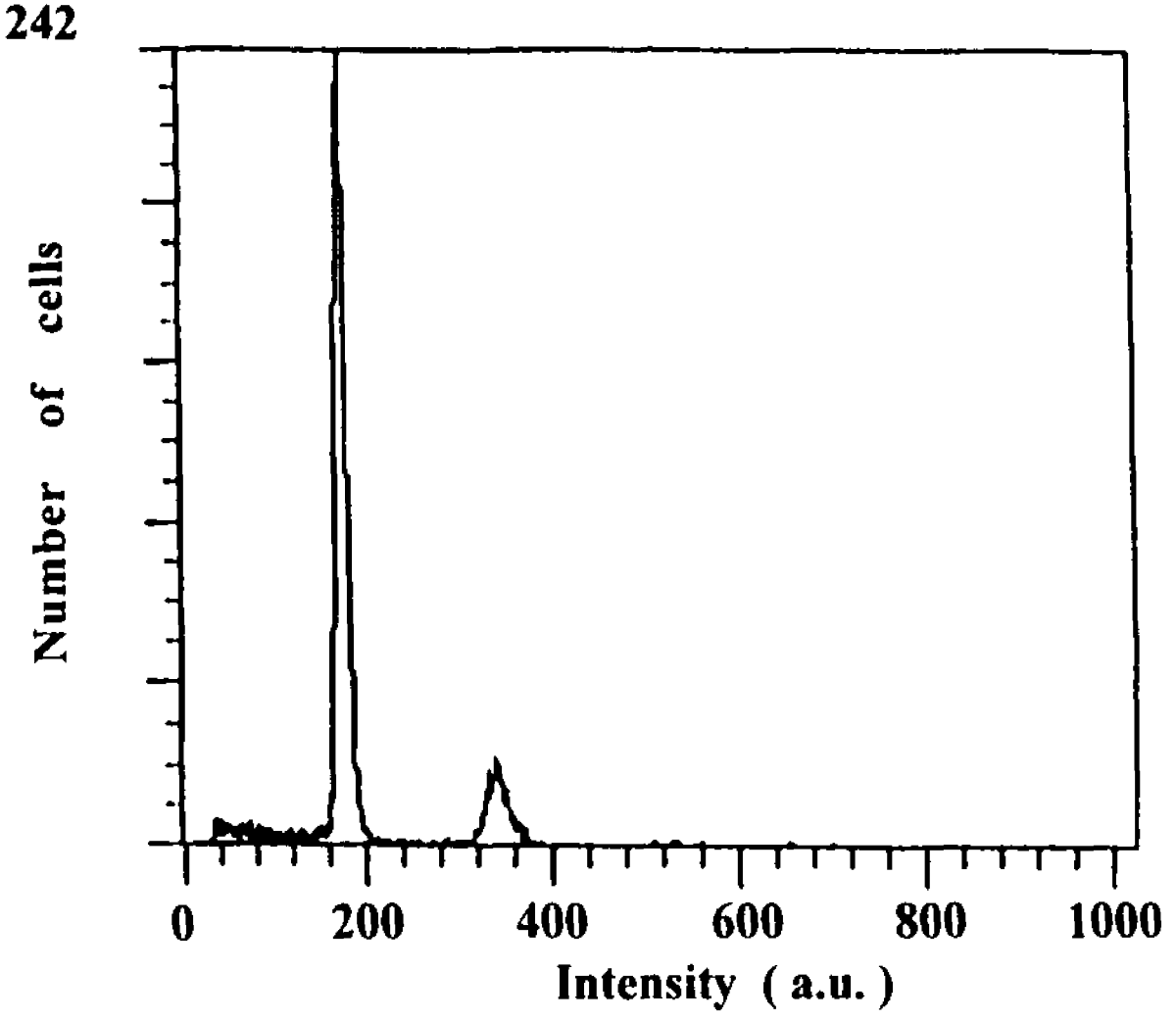

Fig. 4.4(a) Flow cytometry result of number of cells versus fluorescence intensity for breast cancer specimen

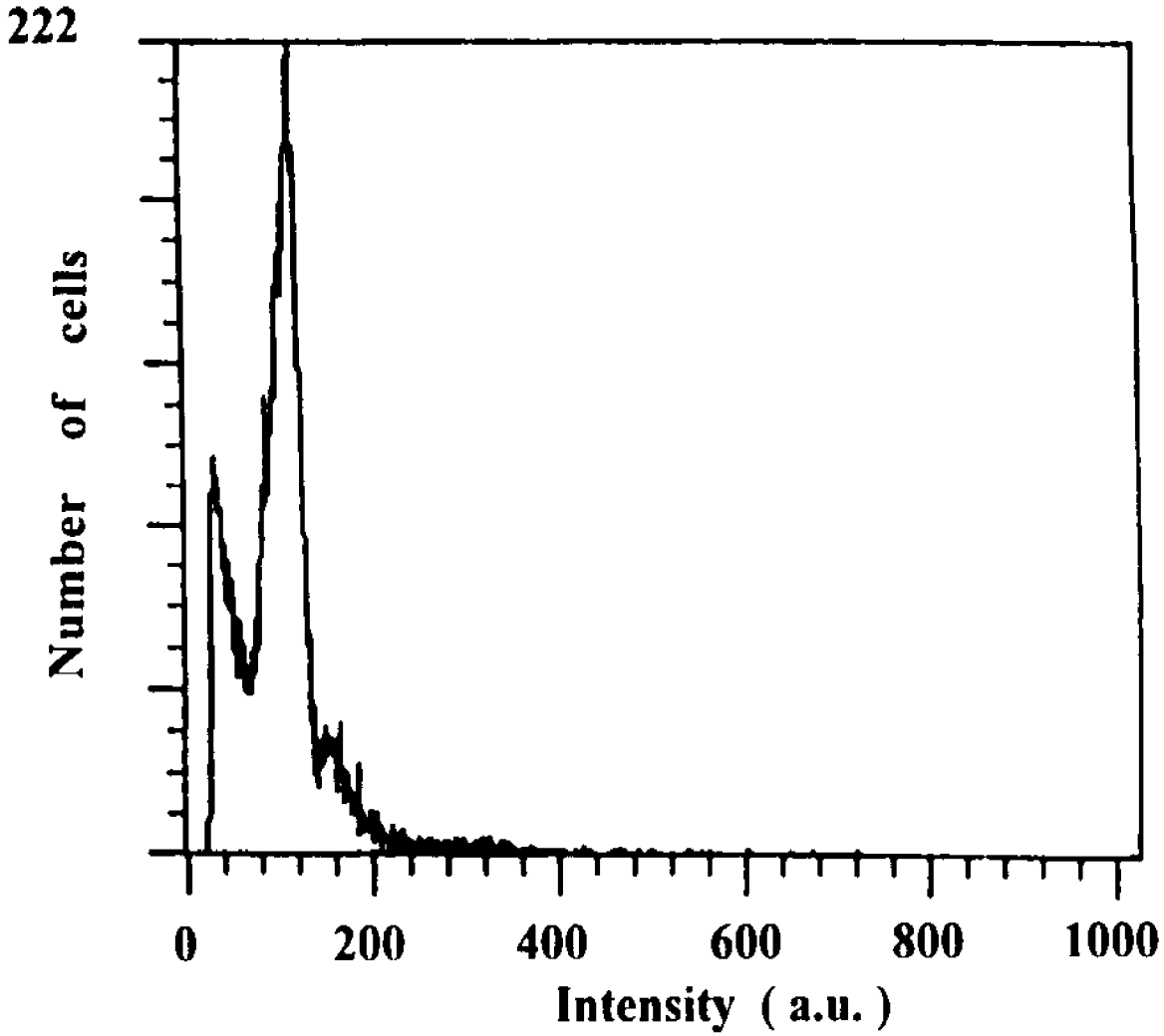

Fig. 4.4(b) Flow cytometry result of number of cells versus fluorescence intensity for colon cancer specimen

V. Summary

An object embedded in a highly random medium cannot be easily observed because multiple light scattering randomizes the signal light direction.[1,2,3] Objects hidden in random scattering media are common in nature, and developing a simple technique to see such hidden objects is important for many field. In medicine, for example, it is highly desirable to image the tumor hidden in a breast by using light instead of x rays. An optical imaging method called transillumination or diaphanography[4-6] has been developed. In this method light is incident upon the breast, and the transmitted light is measured. A shadow of the tumor may be observed because the absorption and scattering characteristics of the tumor are different from those of the normal tissue. Typically, a tumor of 1-cm diameter[4,5] can be detected. However, multiple light scattering in the breast blurs the image and may result in making the tumor unrecognizable, especially when the tumor is too small or lies too deep in the breast. Recently, ultrafast laser technology was used to enhance the image by time gating the ballistic component of the laser pulses and eliminating the diffuse pulse from detection. This time-gating technique has been used by various groups[7-9] to enhance the image of an object hidden in the random medium. Unlike the conventional techniques, a novel imaging technique, fluorescence -absorption technique, is studied to enhance the quality of an image of an object hidden in a highly scattering medium. In this technique, the object is made luminous, and its luminescent light is selected for imaging while the illuminating light is filtered out. The quality of the image can be further improved by selecting the portion of the luminescence spectrum that is strongly absorbed by the random medium.

The absorption, fluorescence, and excitation spectra of a dye in a highly scattering random medium are studied experimentally. The intrinsic

absorption spectrum of the dye does not change in the presence of scatterers, but the presence of scatterers in the media will change the observed fluorescence spectra. The observation is accounted for by the change in photon trajectory path length for the fluorescence emission.

Compared with the current clinically employed flow cytometry technique, quantitative fluorescence image analysis technique is studied. In this technique, the laser-excited fluorescence microscope system enables us to image the biological cells, and analyze its DNA histogram with a better signal to noise ratio in comparison with microscopy using conventional light source. Besides the intensity histogram analysis, It also has the advantage of the ability to analyze the size, shape and DNA distribution of the cells.

REFERENCES

1. A.Ishimaru, Appl. Opt. 17, 348 (1978).
2. A. Ishimaru, Y. Kuga, R.L.T. Cheung, and K. Shimizu, J. Opt. Soc. Am. 73, 131 (1983).
3. K.M. Yoo and R.R. Alfano, Opt. Lett. 15, 320 (1990).
4. R. Lafrenuere, F.S. Ashkar, and A.S. Ketcham, Am. Surg. 52, 123 (1986).
5. E.A. Sickles, Recent Results Cancer Res. 105, 31 (1987).
6. D.S. Dilworth, E.N. Leith, and J.L. Lopez, Appl. Opt. 29, 691 (1990).
7. S. Andersson-Engels, R. Berg, S. Svanberg, and O. Jarlman, Opt. Lett. 15, 1179 (1990).
8. H. Chen, Y. Chen, D. Dilworth, E. Leith, J. Lopez, and J. Valdmanis, Opt. Lett. 16, 487 (1991).
9. J.C. Hebden, R.A. Kruger, and K.S. Wong, Appl. Opt. 30, 788 (1991).

VI. Future research directions

In this thesis work, we have developed a new imaging technique to see an object hidden in scattering media and approach which uses quantitative fluorescence imaging analysis technique to analyze the cancer cells. Much more studies are needed to develop and improve the imaging techniques used in cancer cell's diagnosis.

Malignant cells are often characterized by deviations in their DNA contents from normal healthy cells.[1,2] A relative determination of the amount of DNA in cell is possible by sensitizing the cells by chromophor DNA tags such as dye molecules. The stained cells will fluoresce upon laser excitation. The integrated fluorescence from a cell is expected to be proportional to the amount of DNA materials within a cell. The fluorescent image of a cell can then be acquired using a microscope and high resolution color CCD camera and digitally recorded using a PC computer equipped with a color frame - grabber and appropriate software. The cell fluorescence collected by the microscope can also be analyzed by an optical spectrum multi-channel analyzer and the spectral distribution of the fluorescence acquired together with the spatial image. Thus, it is possible to compare normal healthy cells and malignant cancerous cells not only using the integrated fluorescence distributions from normal and cancerous samples but by size, shape, texture analysis, DNA distribution maps within the individual cells, and possible deviations of spectral information. We also foresee future applications of our system in Raman microspectroscopy, polarized light microscopy in combination with spatial filtering for three dimensional imaging of opaque specimen, etc.

Further development of this technique for actual clinical use will include development of neural network algorithms trained on accumulated data sets which can run real time diagnostics on acquired images from a set of cell,

sorting them into malignant/nonmalignant groups.

REFERENCES

1. P.S. Oud, A.G.J.M. Hanselaar, M.M.M. Pahlplatz, J.W.R. Meijer, and G. Peter Vooijs, Appl. Opt. 26, 3349 (1987).

2. Marluce Bibbo et. al., "Computed cell Image Information", Monogr. Clin.Cytol.Vol.9, pp 62-100 (1984).

BIBLIOGRAPHY

Ahmed, S.A., Z.W. Zang, K.M. Yoo, M.A. Ali, and R.R. Alfano, Appl. Opt., Vol. 33, No. 13, 2746-50(1994).

Andersson-Engels, S., R.Berg, S.Svanberg, and O.Jarlman Opt.Lett.15,1179(1990).

Bakhshiev, N.G., Opt. Spectrosc. Vol 32, PP. 1151 (1972).

Bakhshiev, N.G., and B.S. Neporent, Opt. Spectrosc. Vol. 16, pp. 191(1970).

Baltes, H.P.ed., Inverse Source Problems in Optics (Springer-Verlag, Berlin,1978).

Bibbo, M., et. al., "Computed cell Image Information", Monogr. Clin.Cytol.Vol.9, pp 62-100 (1984).

Born, M., and E. Wolf, Principles of Optics, 4th Edition, (Pergamon, New York,1970), 633-664.

Chen, H., Y.Chen,D.Dilworth,E.Leith,J.Lopez, and J.Valdmanis, Opt.Lett.16,487 (1991).

Dainty, J.C.ed., Laser Speckleand Related Phenomena (Springer Verlag, Berlin, 1975), pp 203-278.

Debiasio, R., G.R.Bright et al., J. Cell Bio. 105,1613(1987).

Debye, P., Ann. Physik. 30, 59 (1909).

Dilworth, D.S., E.N.Leith, and J.L.Lopez, Appl.Opt.29,691(1990).

Dressler, L.G., and Sue A. Bartow, Seminars in Diagnostic Pathology, Vo l6, Nol (February) 1989: pp55-82.

Hebden, J.C., R.A.Kruger, and K.S.Wong, Appl.Opt.30,788(1991).

Ho, P.P., P.Baldeck,K.S.Wong,K.M.Yoo,D.Lee, and R.R.Alfano, Appl.Opt.28,2304(1989).

Horecker, B.L., "The absorption spectra of hemoglobin and its derivatives in the visible and near infra regions," J. Biol. Chem. 148, 173-183 (1943).

Hufnagel, R.E., and N.R.Stanley, J.Opt.Soc.Am.54,52(1964).

Ishimaru, A., Wave propagation and scattering in random media, Vol. 1& 2,(Academic Press, New York, 1978).

Ishimaru, A., Appl.Opt.17,348(1978).

Ishimaru, A., Y.Kuga, R.L.T.Cheung, and K.Shimizu, J.Opt. Soc.Am.73,131(1983).

Jaskson, J.D., Classical Electrodynamics, 2th Edition, (Wiley, New York, 1975).

Kopeika, N.S., J.Opt.Soc.Am.72,548(1982).

Kopeika, N.S., J.Opt.Soc.Am.72,1092(1982).

Kuga, Y., and A.Ishimaru, J.Opt.Soc. Am. A2,2330(1985).

Lafrenuere, R., F.S.Ashkar,and A.S.Ketcham, Am.Surg.52,123(1986).

Lee, B.R., B.D.Haseman, C.P.Reynolds, Cytometry 10,256(1989).

Liu, F., K.M.Yoo, and R.R.Alfano, Opt.Lett.16,351,(1991).

Lockett, S.J., K.Jacobson et al., Biotechniques 10,514(1991).

Lutomirski, R.F., and H.T.Yura, J.Opt.Soc.Am.61,482(1971).

Martorell, J., and N.M. Lawandy "Spontaneous emission in a disordered dielectric medium". Phys. Rev. Lett. 66, 887-890 (1991).

Mie, G., Ann. Physik. 25, 377 (1908).

Montan, S., and L.G. Stroemblad, "Spectral characterization of brain

tumors utilizing laser-induced fluorescence," Lasers Life Sci. 1, 275-285 (1987).

Oud, P.S., A.G.J.M. Hanselaar, M.M.M. Pahlplatz, J.W.R. Meijer, and G. Peter Vooijs, Appl. Opt. 26, 3349 (1987).

Parry, W.L., et al., "Cancer detection by quantitative fluorescence image analysis", The J.of Urology, Vol.139, 270-274 (1987).

Sato,S.I. et al., "Highly sensitive fluorescence microscope system for single biological cell using laser excitation and digital image processing and display",Opt.Quantum Electronics, V. 18(1), 81-84 (1986).

Shafer, F.P., W. Schmidt, and J. Volez Vol. 9, pp. 306-309, October (1966).

Shapiro, H.M., "Practical Flow Cytometry" (Alan R. Liss, Inc., New York, 1988).

Sickles, E.A., Recent Results Cancer Res.105,31(1987).

Sorokin, P.P., and J. R. Lankard, IBM J Research and develop. Vol. 10, pp. 162-163, March (1966).

Sorokin, P.P., and J. R. Lankard, IBM J. Research and Develop. Vol.11, pp. 148, March (1967).

Spaeth, M.L., and D. P. Bortfield, Appl. Phys. Letters, Vol. 10, pp. 179-181, September (1966).

Tam, W.G., and A.Zardecki, Int.J.Infrared Millimeter Waves, 6249 (1985).

Tata, D.B., M. Foresti, J. Cordero, P. Tomashefsky, M.A. Alfano, and R.R. Alfano,"Fluorescence polarization spectroscopy and time-resolved fluorescence kinetics native cancerous and normal rat kidney tissues," Biophys.J.Biophys.Soc.50, 463-469 (1986).

Van de Hulst, H.C., Light Scattering by Small Particles, (Dover, New York, 1981).

Wang, L.M.,Y.Liu,P.P.Ho, and R.R.Alfano,"Ballistic imaging of biomedical samples using picosecond optical Kerr gate," in Proceedings of OE LASER'91: Symposium on Biomedical Optics (Society of Photo-Optical Instrumentation Engineers, Bellingham, Wash.). Wells, W., J.Opt.Soc.Am.59,686(1969).

Wick, R.A., Appl.Opt.26.3210 (1987).

Yang, Y.L.,Y.M. Ye, R.M. Li, Y.F. Li, and P.Z. Ma, "Characteristic autofluorescence for cancer diagnosis and its origin," Laser Surg. Med. 7, 528 (1987).

Yoo, K.M., and R.R.Alfano, Opt.Lett.15,320(1990).

Yoo, K.M., F. Liu, Z.W.Zang, S.A. Ahmed, and R.R. Alfano, "Absorption and fluorescence-absorption techniques for imaging through a scattering medium", SPIE, Vol. 1599, Recent Advances in the Use of Light in Physics, Chemistry, Engineering and Medicine 323/1991.

Yoo, K.M., Z.W. Zang, S.A. Ahmed, and R.R. Alfano, "Imagine objects hidden in scattering media using a fluorescence-absorption technique", Opt.Lett.16,1252-54 (1991).

Zardecki, A., S.A.W.Gertl, and J.F.Embury, Appl.Opt.23,4142(1984).